Technical University of Denmark

DTU

Validation of the NewGust approach

Larsen, Gunner Chr.

Publication date:
2003

Document Version
Publisher's PDF, also known as Version of record

Link back to DTU Orbit

Citation (APA):
Larsen, G. C. (2003). Validation of the NewGust approach. (Denmark. Forskningscenter Risoe. Risoe-R; No. 1221(EN)).

DTU Library
Technical Information Center of Denmark

Validation of the NewGust Approach

Gunner Chr. Larsen

Abstract

The gust events described in the IEC-standard are formulated as coherent gusts of an inherent deterministic character, whereas the gusts experienced in real situation are of a stochastic nature with a limited spatial extension. This conceptual difference may cause substantial differences in the load patterns of a wind turbine when a gust event is imposed.

Methods exist to embed a gust of a prescribed appearance in a stochastic wind field in a consistent way. The present report deals with the verification of a synthetic wind field resulting from such a model - the NewGust model. The NewGust model is restricted to gust events associated with the longitudinal turbulence component, and consequently no attention is paid to wind direction gusts.

The verification is performed by analysing existing measurements of wind speed gust situations and associated structural loads on a Vestas V39 turbine, and subsequently to compare these with analogues simulations established by applying the NewGust method to establish a (synthetic) gust loading. Eight load cases, representing four mean wind speed regimes that reflect different control characteristics, have been analysed. Attention has been paid to select the largest possible gust events, associated with each of the mean wind ranges, within the available data material.

The work reported makes part of the project "Modelling of Extreme Gusts for Design Calculations " (NEWGUST), which is co-funded through JOULEIII on contract no. JOR3-CT98-0239.

Contents

1. Background

The work reported makes part of the project "Modelling of Extreme Gusts for Design Calculations " (NewGust), which is co-funded through JOULEIII.

In essence the NewGust method, describes a way to combine a stochastic turbulence field (as presently used for fatigue analysis) and a well defined deterministic gust shape (which can be theoretically derived) in such a way that a realistic extreme gust is obtained. The project approach can be divided into the following steps:

1) Experimental verification of the shape of extreme gusts. From theory it follows that the gust shape resembles the autocorrelation function of turbulence. This will be verified by comparing with shapes extracted from an existing database of wind measurements.
2) Determination of the probability distribution function of extreme gusts from a database of wind measurements and/or from theory (in case wind measurements are not available for a long enough period).
3) Development of an advanced method to determine the dynamic response of a wind turbine to extreme gusts. The advanced method will generate wind time series, which can not, in a statistical sense, be distinguished from natural extreme wind gusts.
4) Implementation of the advanced method in a number of existing design packages.
5) Experimental verification of the predicted loading and response of a wind turbine to extreme gusts.

The present report deals with item 5) of the tasks described above.

2. Introduction

Extreme load cases have obtained increasing attention in the efforts with establishing rational design guidelines for wind turbine structures during resent years. Part of the extreme load cases relates to imposition of wind speed gusts on the wind turbine.

Up to now such gusts has traditionally been described as coherent wind gusts that do not reflect the stochastic nature of the true wind field. This philosophy behind this procedure is therefore not consistent with the conventional treatment of fatigue loading, which is based on a complete tree dimensional spatial description of the turbulence described in terms of its stochastic characteristics (i.e. autospectra and coherence functions). The NewGust method is the acronym of a procedure that allows wind speed gusts with a spatial extension to be embedded in a stochastic wind field. Based on constrained turbulence simulation, the NewGust method offers a convenient short cut of establishing an extreme wind speed gust that would eventually result from a traditional wind field simulation, if the simulation time was specified long enough (of the order of magnitude years and therefore unrealistic in any practical application).

The constrained simulation is based on a theoretical description of a mean gust shape, obtained from level crossing statistics, in combination with an algorithm for embedding a gust in a stochastic turbulence environment, that in average will reflect the derived mean gust shape. Previous reports have described the derivation and verification of the theoretical mean wind speed gust shape [1], and the implementation of the NewGust method in traditional turbulence generators [14]. The present report deals with the synthesis of these tasks and aims at an overall verification of the method.

The verification is performed by analysing existing measurements of wind speed gust situations and associated structural loads on a Vestas V39 turbine, and subsequently to compare these with analogues simulations achieved using the NewGust method to establish a (synthetic) gust loading.

Based on control system considerations four different mean wind speed regimes have been selected for the verification – a low and medium mean wind speed in the wind speed range where the pitch control is not active, the nominal mean wind speed and finally a high mean wind speed in the range of the cut-out wind speed. For each mean wind speed regime, the measured and simulated blade root moments and rotor shaft moments have been compared.

3. Available measurements

The available load and wind field measurements originate from the Sky River wind farm situated close to Tehachapi in California, USA. The wind farm consists of 342 Vestas V27 wind turbines and one Vestas V39 wind turbine. The site is characterized by being a very inhomogeneous terrain, which in turn implies severe wind conditions and thereby strong dynamic loads on a wind turbine structure. The measurements were carried out in the period extending from May 17 to June 21, 1993.

The *structural response* of the Vestas V39 turbine has been recorded. The structural measurements comprise recordings of flap- and edge wise blade bending moments, shaft torque and bending moments and tower leg forces (lattice tower). In addition the yaw position, rotor position, electrical output as well as the rotational speed have been recorded. The associated *wind field* measurements consist of recordings from cup anemometers and wind vanes in two heights as well as from sonic anemometers positioned at two other levels. The wind field measurements are scanned with 2Hz, whereas the structural measurements are scanned with 8Hz.

In order to facilitate the data analysis, the wind field measurements as well as the corresponding structural measurements have been implemented in "Database on Wind Characteristics" [3].

3.1 Site description

The Sky River wind farm is situated on ridges in a complex mountainous terrain about 15km northeast of the Tehachapi Pass in California. The topography of the terrain around the wind turbines and the position of the V39 turbine as well as of the meteorological tower are illustrated in Figure 3.1.1 below.
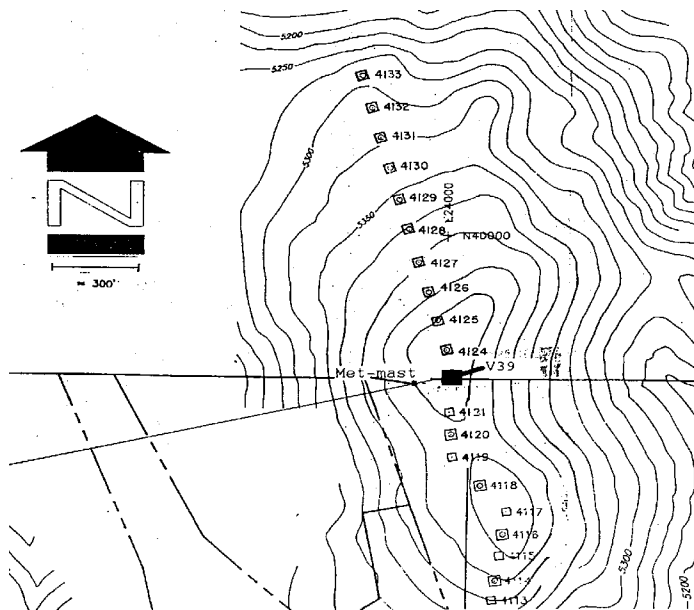

Figure 3.1-1 Site topography and wind farm layout.

The wind climate is thermal driven. The thermal effects are completely dominated by the temperature gradient established between a dessert area east of the site and the open sea west of the site. Caused by differences in the diurnal variation of the heating processes of the air above the dessert and sea, respectively, the resulting wind direction systematically changes 180º twice a day. The prevailing wind directions, as determined from the available measurements, are along the line 73º - 253º, which is approximately perpendicular to the ridge at which the V39 turbine is situated.

The energy resources have been estimated prior to installation of the wind farm by conducting long term wind resource measurements in the period from 1984 to 1988 [6]. These long-term wind measurements have resulted in an estimate of the average annual wind speed at hub height equal to 7.2 m/s [4, 6]. However, due to the topography of the terrain the wind potential may differ significantly even at small distances.

The measured mean annual air density (at 2260m elevation) is equal to 1.040 kg/m^3. In the *summer* period the air density varies between 0.981 and 1.015 kg/m^3. In the *winter* period the air density varies from 1.048 to 1.072 kg/m^3.

3.2 Experimental set-up

Structural measurements on the V39 turbine as well as wind field measurements on a meteorological tower have been performed. As indicated on Figure 3.1-1 the meteorological tower has been erected in the prevailing wind direction in front of the Vestas V39 turbine. The direction from the meteorological tower to the V39 turbine is 78º (cf. Figure 3.1-1).

The objective of the *meteorological measurements* is to provide detailed information of the incoming wind flow to the wind turbine during the load measurements, as the aerodynamic loading constitutes a dominating contribution to the total loading of the wind turbine.

Wind speeds are measured at four levels to determine the turbulence characteristics and the variation of the mean wind speed with height (the mean wind shear). In addition wind directions are measured at the same four levels in order to determine the yaw characteristics of the wind turbine. Further also recordings of the air pressure and temperature are performed in order to make a determination of the air mass density possible. The instrumentation of the meteorological tower is specified in Table 3-2.1.

No.	Wind field parameter	Sensor
1	Wind speed 40.9 m (hub)	Risø cup-anemometer Reg.0218/0058
2	Wind direction 40.9 m	Risø wind vane Reg.0107/0110
3	Temperature 40.9 m	Pt100 P1182/P1983C Reg.0118/-
4	Temperature diff. 10.7 m/40.9 m	Pt100 P1182/P1348A/P1983C Reg.0028/0132/-
5	Wind speed 10.7 m	Risø cup-anemometer Reg.0220/0067
6	Wind direction 10.7 m	Risø wind vane Reg.0108/0119
7	Sonic u_x (u) 42.7 m	Gill sonic u_x Reg.0061/0064
8	Sonic u_y (v) 42.7 m	Gill sonic u_y Reg.0061/0064
9	Sonic u_z (w) 42.7 m	Gill sonic u_z Reg.0061/0064
10	Sonic u_x (u) 19.3 m	Gill sonic u_x Reg.0062/0065
11	Sonic u_y (v) 19.3 m	Gill sonic u_y Reg.0062/0065
12	Sonic u_z (w) 19.3 m	Gill sonic u_z Reg.0062/0065
13	Air pressure (tower bottom)	Vaisala, Reg.0444

Table 3.2-1 Instrumentation of the meteorological tower.

The objective of the *structural measurements* is to provide detailed information of the structural dynamic load process of different wind turbine components (blade, rotor). The measurements are mainly concerned about the load process associated with normal operation, but also a few stand still situations have been recorded.

The structural response (of relevance for the present analysis) is recorded in terms of torque and/or bending moments in blade- and main shaft cross sections. The investigated blade cross section is positioned close to the blade flange at r=0.85m measured from the hub center along the blade axis. Flapwise as well as edgewise bending moments have been recorded. The main shaft cross section is positioned at l=0.8m measured from the hub center along the main shaft axis. The main shaft measurements include bending moments (in two mutual perpendicular directions) as well as torque.

The main shaft bending moments have subsequently, together with the rotor position recording, been used to determine synthetic time series describing the rotor yaw- and tilt loading (at the position of the recording of the rotating shaft bending moments). Note, that for this transformation to be meaningful it is essential to compensate for possible drift in the mean signals (the mean rotational shaft bending moment is required to have zero mean) and further to ensure that the two involved rotating bending moments exhibits the same standard deviation.

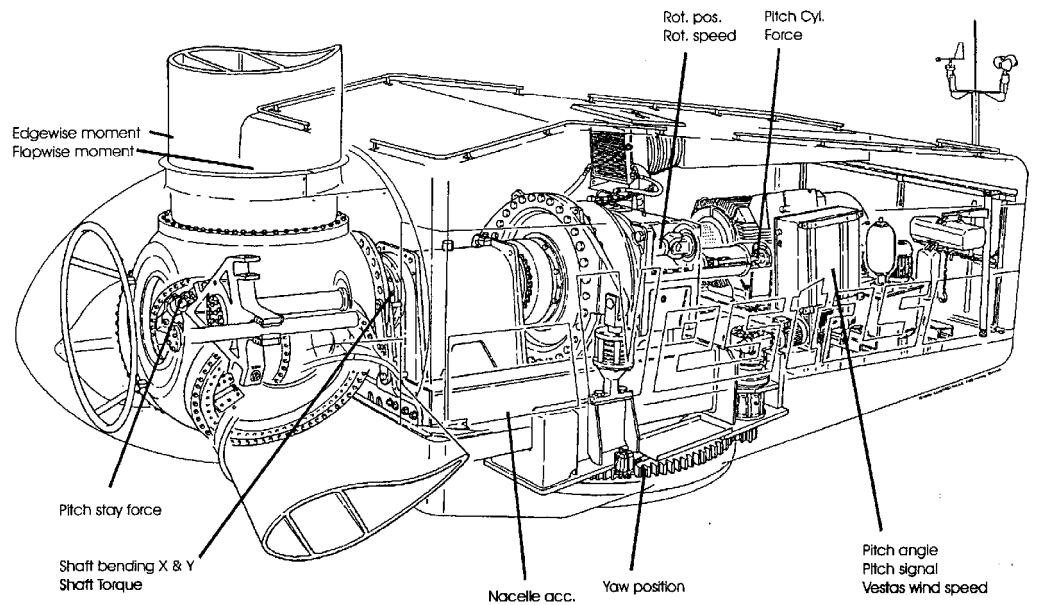The instrumentation of the Vestas V39 turbine is illustrated on Figure 3.2-1.

Figure 3.2-1 Instrumentation of the V39 turbine.

The detailed information on sensor types and sensor positions appears from table 3.2-1.

No.	Wind turbine parameters	Sensor
1	Flapwise bending moment	Strain gauge (full bridge on blade root at r=0.85m)
2	Edgewise bending moment	Strain gauge (full bridge on blade root at r=0.85m)
3	Shaft bending moment (M_x)	Strain gauge (full bridge on main shaft at l=0.8m)
4	Shaft bending moment (M_y)	Strain gauge (full bridge on main shaft at l=0.8m)
5	Rotor torque	Strain gauge (full bridge on main shaft at l=0.8m)
6	Electrical Power	Current transformer, power converter
7	Yaw moment	Calculated from the shaft bending and rotor position
8	Tilt moment	Calculated from the shaft bending and rotor position
9	Rotor position	
10	Yaw position	
11	Pitch angel	Voltage signal from the control system

Table 3.2-2 Instrumentation of the Vestas V39 turbine.

3.3 General wind field characteristics

In order to facilitate the best possible simulation of the measured wind fields, the meteorological and structural measurements have been used to quantify the overall wind climate on the site in terms of statistical measures including mean values as well as spectra [4], [5], [7]. This part of the analysis has concentrated on measures that are hard to access with sufficient statistical significance from only a single 10-minute time series.

The analysis comprises the *mean wind* profile (streamline inclination and vertical wind shear including speed up effect), general *turbulence characteristics* (turbulence length scales, coherence decay factors and relations between longitudinal-, lateral- and transversal turbulence intensities) and air mass density.

Streamline inclination

The effect of site topography on the inclination of the mean wind speed flow is evaluated by analysis of the sonic measurements at 19.3m and at 42.7m, respectively. Two wind direction sectors have been investigated – sector 1 (234º-254º) and sector 2 (254º-274º). The average streamline inclination associated with sector 1 is 8.6º at level 19.3m and 5.5º at level 42.7m. As expected the inclination is observed to decrease with altitude and to be independent of the mean wind speed. The corresponding values for sector 2 are 8.8º and 6.7º. The variability inherent in this kind of investigations is illustrated in Figure 3.3-1 showing the streamline inclination associated with sector 1 at level 42.7m.
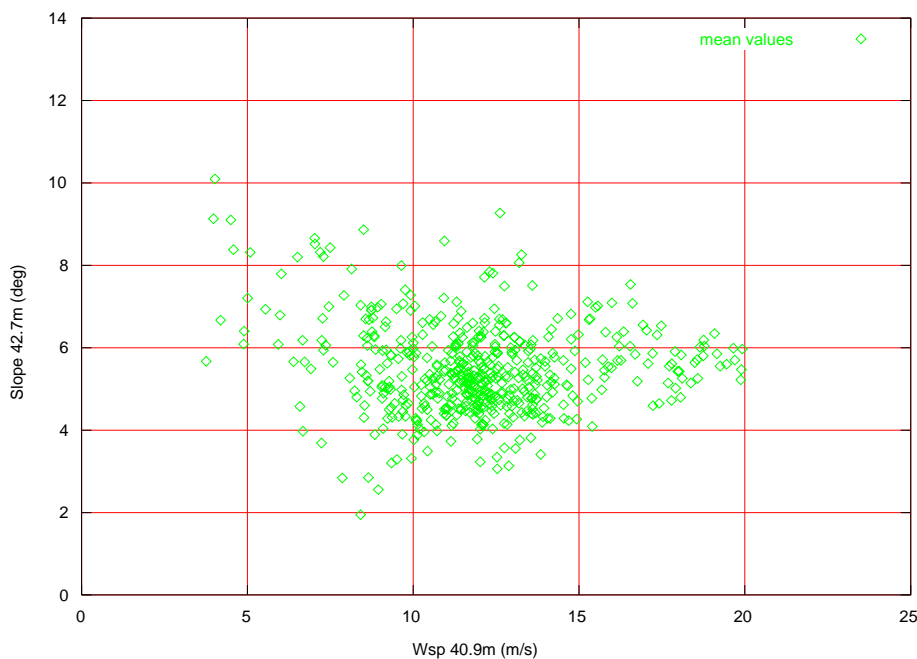

Figure 3.3-1 Streamline inclination angle at 42.7m versus wind speed at 40.9m (sector 1).

Speed up effect

From general investigations of flow over simple 2-dimensional hills, speed up effects close to the top of the hill is well known [8]. In the present situation, the meteorological measurements do not indicate such a phenomenon (cf. Figure 3.3-2). However, a detailed analysis of azimuthally binned simulated and measured flapwise loads reveal that such a phenomenon is indeed present [7]. The investigations show that simulations associated

with the wind shear profile, as estimated from the meteorological measurements, strongly overestimates the flapwise loading above hub height compared to the structural measurements. The discrepancy is believed to be caused by a substantial modification of the wind shear profile at the position of the V39 turbine. The turbine is positioned somewhat closer to the top of the hill that the meteorological tower, which explains that the speed up effect is hardly visible at the location of the meteorological sensors.

By tuning the form of the vertical wind shear until agreement is obtained between simulated and measured azimuthally binned flapwise loads, an estimate of the vertical wind profile at the position of the V39 turbine can be obtained. The result [7] is given in Figure 3.3-2 for the hub mean wind speed equal to 12.3m/s as measured on the meteorological tower.
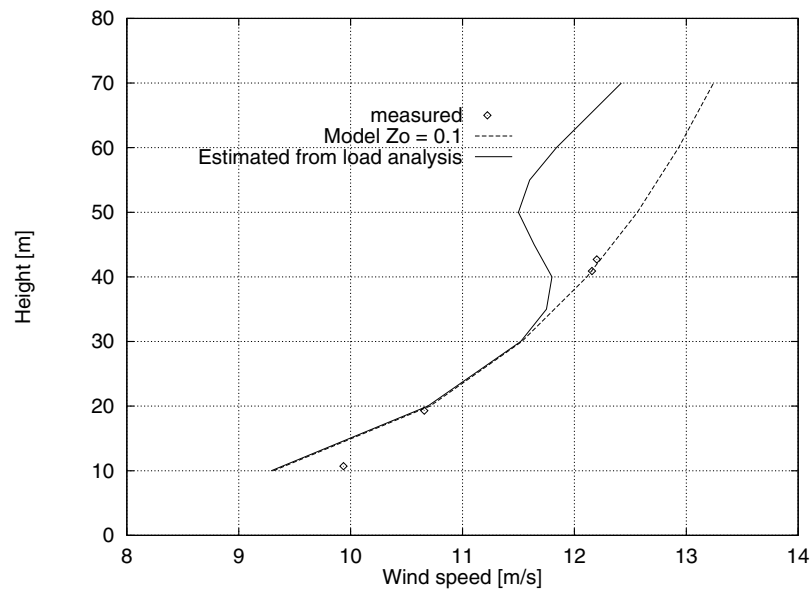

Figure 3.3-2 Speed up effect estimated for hub mean wind speed equal to 12.3 m/s. (taken from [7]).

Turbulence intensities

In [4], the standard deviations of the lateral (σ_v) and transversal (σ_w) turbulence components have been compared with the standard deviation of the longitudinal turbulence component (σ_u). The analysis is based on the sonic measurements performed at 19.3m and at 42.7m. The result is that the magnitudes of σ_v/σ_u and σ_w/σ_u are independent of the mean wind speed and equal to 1.05 and 0.8, respectively. This is in contrast with conventional values associated with homogeneous terrain (typically 0.8 and 0.5, respectively).

Turbulence length scale

In [7] the turbulence spectra have been found to be well described by a Kaimal type of spectrum. For the analysed time series, longitudinal turbulence length scales are found to be in the range 600m-800m, the lateral length scale in the range 250m-500m and the transversal length scale in the range 150m-250m.

Coherence

An analysis of the coherence of the wind speed components has been conducted in [7] based on a relatively large amount of data. Neglecting cross correlation between different turbulence components and using a simple Davenport like coherence model, the coherence

decay factors have been estimated to 12 for the longitudinal turbulence component, 7 for the lateral turbulence component and 5 for the transversal turbulence component.

Air mass density

The measured mean air density in 2260m elevation has been determined to 1.040 kg/m³ [4]. In the summer period the air density varies in the range from 0.981 to 1.015 kg/m³. In the winter period the air density varies in the range from 1.048 to 1.072 kg/m³.

3.4 Selection of data

With the purpose of verifying the NewGust method through comparison of simulations and measurements, a number of interesting gust load situations has been selected among the available wind field data. For a pitch controlled wind turbine the severity of a gust load relates to the gust amplitude as well as to the gust rise time (compared to the time constant inherent in the pitch regulation algorithm). The latter dependence relates of course to turbines in normal operation. Resent investigations, however, show that the extreme loading during operation is more severe that extreme loading at stand still [9], and the present investigation is therefore restricted to gust loading on turbines in normal operation only.

From the theoretical mean gust shape expression derived in [1] it is seen that the gust time gradient is increasing with increasing gust amplitude when strictly monotonously autocorrelation functions are assumed. For mean gust shapes extracted from measurements this tendency may be even more pronounced as predicted by the theory [1]. As a consequence the present verification concentrates on large gust amplitudes only.

The available sizes of wind speed gust amplitudes, expressed as gust amplitudes normalised with the standard deviation of the wind speed, is illustrated in Figure 3.4-1 as function of the mean wind speed. The data has been extracted by establishing a data search profile in "Database on wind Characteristics" [3] and relates to the wind direction sector 180°-345°, where no wake situations exist and where the meteorological tower is positioned upstream relative to the wind turbine. As seen (and expected from theory) no trend of gust size as function of the mean wind speed is observed.
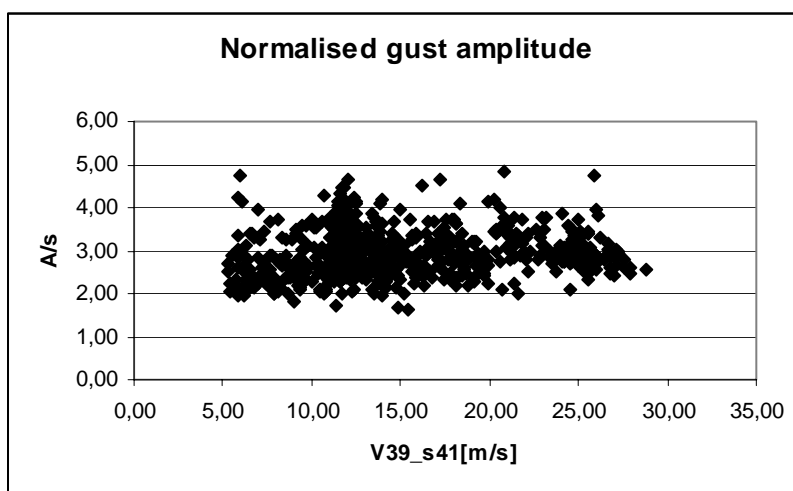

Figure 3.4-1 Gust amplitudes as function of mean wind speed.

The effect of gust rise time (for a pitch regulated turbine) on the load response depends on the operational conditions of the control system. In Figure 3.4-2 the mean pitch angle has

been plotted as function of the mean wind speed for the V39 turbine using data from [3]. The data reflects different "classes" of pitch angle response, on a given change in the wind speed conditions, depending on the wind speed regime. For the present analysis four mean wind speed regimes have been defined:

1. A low wind speed regime with a moderate negative pitch angle gradient with respect to wind speed increments;
2. A medium wind speed regime characterized by passive pitch control;
3. A nominal wind speed regime with a large positive pitch angle gradient with respect to wind speed increments (and thus substantial response times of the pitch system); and
4. A high wind speed regime characterized by medium positive pitch angle gradient with respect to wind speed increments.
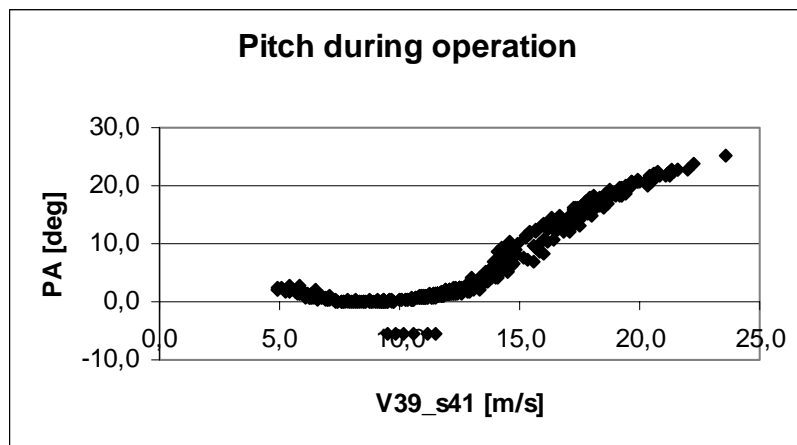
Figure 3.4-2 Pitch angle as function of mean wind speed at hub height for the V39 turbine.

Based on the above considerations, it was decided to let each of the defined wind speed regimes be represented by *two* time series in the analysis. In the selection of suitable time series, normal operation of the V39 turbine has been a precondition. The main characteristics of selected time series for the NewGust validation are summarised in Table 3.4-1.

Load case	V[m/s]	TI [%]	Gust Ampl. [A/s]	Yaw-err.[deg]	Incl. [deg]	Quantile [%]
1	6.07	15.0	4.15	-1.7	8.4	97
2	5.97	12.1	4.76	-6.3	8.3	99
3	11.96	6.0	4.01	-9.6	8.4	96
4	11.99	4.6	4.65	-12.5	8.4	99
5	13.84	10.8	4.10	-8.1	8.4	97
6	16.20	16.4	4.50	-10.5	8.7	99
7	20.63	9.8	4.01	-6.7	8.7	96
8	17.22	13.0	4.66	-7.5	8.7	99

Table 3.4-1 Basic characteristics of gust time series.

The quantile specification given in Table 3.4-1 refers to an estimated (normalised) extreme wind speed gust probability density function based on (normalised) extreme gusts extracted from all available 10-minute time series (and thereby with a recurrence period of 10 minutes). The fact that no trend with mean wind speed was observed in Figure 3.4-1 justifies that the probability density function is not conditioned on the mean wind speed.

The extreme gust distribution turned out to be well represented by an EV1 distribution expressed by:

$$f(A/s; \alpha, \beta) = \alpha \exp[-\exp[-\alpha(A/s - \beta)]] \exp[-\alpha(A/s - \beta)] \quad ,$$

where A/s denotes the normalised extreme gust size and (α, β) are the distribution parameters which have been estimated to (2.37,2.68). The resulting estimated extreme value distribution is illustrated in Figure 3.4-2.
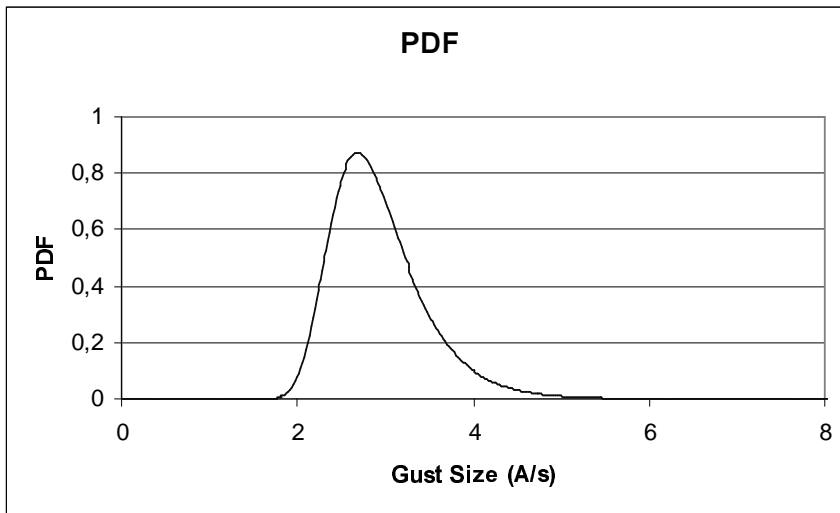

Figure 3.4-3 Estimated extreme probability density function of normalised wind speed gusts.

The selected wind speed time series as measured in hub height are shown in Appendix A together with a specification of the time of the occurrence of the selected extreme gust.

4. Simulations

In order to verify the gust model described in [1] and [14], two aeroelastic models of the pitch controlled wind turbine Vestas V39 are established – one based on the HawC package and the second based on the FLEX4 package. The aeroelastic code HawC [10] is developed at Risø, whereas FLEX4 [12] is developed at DTU. Risø has performed the HawC simulations, whereas Vestas Wind Systems A/S conducted the FLEX4 simulations.

The applied aeroelastic models differ slightly from a traditional V39 aeroelastic model, as the gear ratio is increased and the tower shadow description is modified. The gear ratio is increased in order to reflect a 1800 rpm generator (contrary to a conventional 1500 rpm generator) due to the higher grid frequency in U.S.A. compared to Europe. The rotor rotational speed is related to the aerodynamic performance and is therefore identical to the traditional rotational speed. The tower shadow model has been modified in order to account for the lattice tower construction used for the turbines erected at the Sky River site.

The turbulence wind field input, for both aeroelastic codes, was supplied by the turbulence generator Sosisc [11] with a constraint simulation algorithm implemented. The eight measured wind speed gust load cases, as defined in Chapter 3, have been simulated, and the wind turbine responses have subsequently been compared with the analogues measured signals.

4.1 Description of the V39 turbine

The Vestas V39 turbine is a pitch controlled, three bladed, upwind and constant speed turbine with an active yaw mechanism. It has a rotor diameter of 39m, a hub height of 41.4m, and a rated power equal to 500kW. The detailed technical specifications used in the aeroelastic model are given in Table 4.1-1.

Rotor

Power regulation:	Pitch
Number of blade :	3
Roter diameter:	39.0m
Swept area:	1195m^2
Hub height:	41.4
Tilt:	5°
Rotor rotational speed:	30 rpm
Blade tip angle:	0° - 90° during operation

Blades

Blade make:	Vestas
Spar and shell material:	GRP
Total blade length:	19.0m
Profiled blade length:	16.5m
Root chord:	1.6m
Blade twist:	15.0°
Blade profile:	NACA 63-200 and FFA-W3

Gearbox

Make:	Flender
Ratio:	1:60

Generator
Make: Siemens
Rated power: 500kW
Voltage: 480VAC
Frequency: 60Hz
Rotational speed:

Lattice Tower
Height: 40.0m

Control system
Make: Vestas

Weights
Blade: appr. 1100kg
Rotor inc. hub: appr. 6300kg
Nacelle ex. rotor: appr. 17300kg
Lattice tower   appr. 18500kg
Total: appr. 42500kg

Table 4.1-1Technical specifications of the Vestas V39 wind turbine

4.2 The HawC model

The structural model is based on 2-node prismatic beam elements with 6 degrees of freedom at each node, corresponding to 3 translations and 3 rotations. The interpolation functions are polynomials of 3rd order, representing the solutions to the equilibrium equations for the element. The wind turbine structure is subdivided into 3 substructures: tower, shaft/nacelle and rotor. The shaft/nacelle and the rotor are described as rotating substructures, coupled to each other and to the tower. An example of a typical division of the wind turbine in finite elements is shown in Figure 4.2-1. A more detailed picture of the division in elements on the blade is shown in Figure 4.2-2.
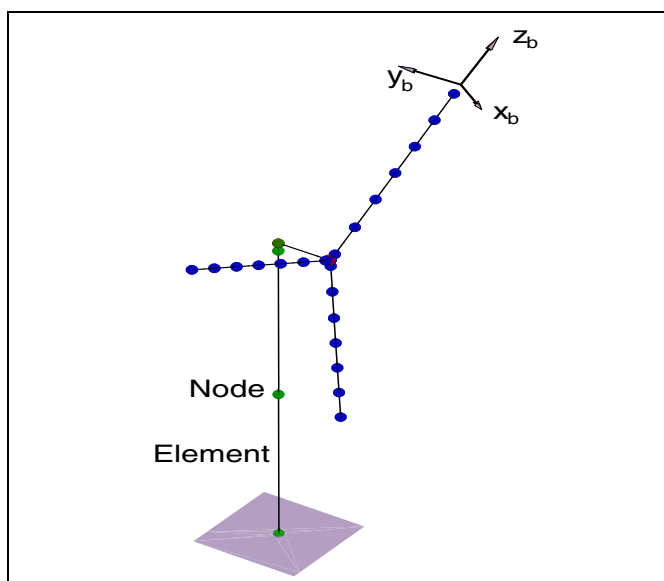
Table 4.2-1 Finite element model of wind turbine.

Real blades are tapered and twisted, whereas the available structural finite elements are prismatic, and the model is thus an approximation. In Figure 4.2-2, a section of the blade is shown in the figure part A and the corresponding model in figure part B, where 2 elements are chosen. The (x_b, y_b, z_b)-coordinate system is a common blade system, with the z_b-axis pointing radially outwards. Each element in B is described in a local element coordinate system - for element no. 'i' the system is denoted (x_{pi}, y_{pi}, z_{pi}) - with the x_{pi} and y_{pi} axes coinciding with the principal bending axes, and the z_{pi} axis coinciding with the elastic axis. The orientation of the local x_{pi} and y_{pi} axis is usually chosen as the orientation of the principal axes at the midpoint of the real element, thus resulting in an approximate description of the structural blade twist. In the figure the z_{pi} axes are assumed to coincide with the common z_p axis, which need not necessarily being the case. In addition to principal bending axes and elastic axis the structural element is described by cross sectional centres for mass and shear.
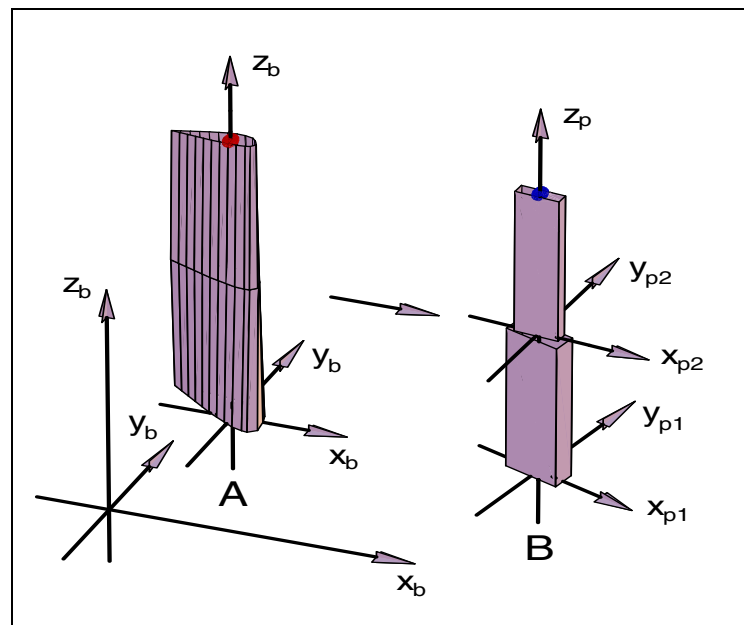
Table 4.2-2 Finite elements of a blade.

For the tower substructure the right hand (x_t, y_t, z_t)-coordinate system is oriented with the y_t-axis pointing in the direction of the mean wind and z_t directed along the gravity force. As for the right handed rotating shaft coordinate system (x_s, y_s, z_s), the y_s coordinate is directed "roughly" in the mean wind direction (except for tilt and taw errors).

The elastic deformations, including rotations, as well as the bearing restrained rotations at the coupling nodes are taken into account in the expressions for the inertia loads on the substructures. Distributed loads on the elements (inertia, aerodynamic and gravity) are consistently transformed to the nodes. This results in a complete coupled dynamic model for response of the wind turbine to external loading described by a set of discrete, non-linear, ordinary differential equations with time varying coefficients.

The flexible elements of the drive train are modelled as shaft elements with mass, structural damping and stiffness. The generator is modelled as a separate rotational degree of freedom with mass moment of inertia and a torque corresponding to the actual generator characteristic, which can be explicitly prescribed in a subroutine.

The pitch control in the model is equivalent to the control on the real turbine; i.e. the blade is pitched both structurally and aerodynamically, controlled by an algorithm identical to the

one applied on the real turbine. Even though the Vestas V39 turbine is a pitch controlled turbine, a simple time-lag stall model is included in the present aerodynamic modelling in order to deal with possible large angles of flow incidence on the inner part of the blades.

The external loading of the structure is caused by aerodynamic loads originating from the fluctuating wind field and by gravity loads. The applied aerodynamic model is the blade element model.

The wind field is composed of a deterministic part (including wind shear, yaw errors, inclination of ground and tower shadow), and a contribution caused by turbulence. The turbulence is generated in a rectangular box with quadratic cross sections in planes perpendicular to the mean wind direction. For the present application of the turbulence generator 16x16 grid points have been specified on a quadratic grid associated with each cross section. The grid points in the rotor plane are equally spaced in both directions. 4096 equally spaced cross sections in the mean wind direction have been applied.

4.3 The FLEX4 model

FLEX4 is an aeroelastic code capable of modelling wind turbines with one, two or three blades. The wind turbines can be fixed or variable speed turbines, and either stall- or pitch regulated. Emphasis have been given to meet a suitable balance between efficiency and accuracy which have resulted in a model with relatively few but essential degrees of freedom (DOF) combined with a fully non-linear calculation of the turbine response, including large rotations from free yaw or teeter. The model is formulated in the time domain, and the modal decomposition technique has been used for the numerical descretization of the equations of motion.

The available DOF's are disposed as follows. Two DOF's are reserved for description of the horizontal deflection (and rotation) of the tower top in (around) two mutually perpendicular directions. One DOF are reserved for describing the tower torsion and the yaw drive flexibility, and one DOF is used to model a tilt rotation simulating the nacelle bedplate flexibility. Three DOF's are used to describe the main shaft flexibility - one accounting for the torsion of the main shaft and two describing the mean shaft bending (or teeter hinges) around two mutually perpendicular directions. The elastic blade deflections are modelled in terms of two flapwise DOF's and two edgewise DOF's. However, only one edgewise DOF (corresponding to the first edgewise bending mode) has been utilised in the present computations. The blades are assumed stiff in torsion. Each blade can be pitched at the root - the pitch angle, however, is not an independent DOF but prescribed by the control algorithm. Finally, the rotor rotation at the position of the front bearing is described by one DOF. Note, that compared to the HawC convention, the sign of the pitch angle and the shaft torsion is reverted in FLEX4.

The aerodynamic loads on the wind turbine blades are calculated using conventional blade element theory. The wind loading include a deterministic component caused by the mean wind field and a stochastic component caused by the turbulence.

The description of the mean wind field includes modelling of mean wind shear, yaw error, terrain inclination and tower shadow. The mean wind shear field is modelled in terms of a conventional power low or, alternatively, prescribed in a table. The tower shadow is approached by approximating the mean wind flow around the tower profile with a two-dimensional potential flow field around an infinite cylinder in case of a tubular tower. In case of a lattice tower, the tower shadow is approximated by modelling the mean wind field as the flow field resulting from a constellation consisting of suitable positioned point sources/sinks in a horizontally uniform flow field (as no flow resistance is introduced, the extend of the wake behind the tower is very limited).

The turbulence is generated in a box with circular cross section in the plane perpendicular to the mean wind direction. For the present application of the turbulence generator 4x32

points are available on the polar grid associated with a particular cross section and 4096 cross sections are equally distributed in the along wind direction. The grid points in the polar grids are equally spaced in the radial as well as in the azimuthal direction.

4.4 Tuning of the structural models

In order to obtain a correct representation of the turbine structural dynamics, the aeroelastic models have been tuned to reproduce the essential natural frequencies obtained from the structural measurements. Usually concentrated masses and distributed masses are known with good accuracy, and therefore the system natural frequencies are fitted by adjusting the elastic properties of the involved components. Both measured and calculated natural frequencies refer to standstill situations with the instrumented blade in a vertically upward position and with the pitch angel equal to 0°. The relevant frequencies are specified in Tables 4.3-1 and 4.3-2 for the HawC and the FLEX4 models, respectively.

Natural frequency	Meas. (Hz)	Calc. (Hz)	Deviation (%)
1. tower bending	0.89	0.88	1.1
1. shaft torsion (drive train)	1.19	1.18	0.8
1. asymmetrical rotor / tower torsion (Yaw)	1.26	1.28	1.6
1. asymmetrical rotor / tower bending (Tilt)	1.55	1.54	0.6
1. symmetrical rotor flapwise	1.78	1.78	0.0
1. asymmetrical rotor edgewise	2.83	2.84	0.3

Table 4.4-1 Measured natural frequencies at standstill with pitch angel 0° as obtained from the HawC model.

Natural frequency	Meas. (Hz)	Calc. (Hz)	Deviation (%)
1. tower bending	0.89	0.91	2.2
1. shaft torsion (drive train)	1.19	1.19	0
1. asymmetrical rotor / tower torsion (Yaw)	1.26	1.26	0
1. asymmetrical rotor / tower bending (Tilt)	1.55	1.50	3.3
1. symmetrical rotor flapwise	1.78	1.78	0
1. asymmetrical rotor edgewise	2.83	2.80	1.1

Table 4.4-2 Measured natural frequencies at standstill with pitch angel 0° as obtained from the FLEX4 model.

As seen the deviation between measured and calculated natural frequencies are very modest, and in this respect the dynamic system behaviour is fully satisfactory.

4.5 Load cases

When simulating wind turbine fatigue loading, the turbulence intensity and the mean wind speed (including description of mean wind speed shear) are the primary parameters, whereas turbulence length scale and coherence decay factors are parameters of secondary importance. The importance of the mean wind speed is further accentuated in the case of skew air inflow on the rotor (either caused by yaw errors or by terrain controlled uphill/downhill flow).

However, when dealing the effects of wind speed gust loads on the structure, the significance of the detailed (time and spatial) structure of the turbulence increases relatively. Consequently, the turbulence length scale and the spatial coherence of the turbulence field must be accessed carefully in order to establish a reliable model of the complete dynamic system under such load conditions.

The presumptions made in order to obtain a reliable simulation of the load cases defined in Section 3.4 are outlined below.

Wind inclination: The present version of the aeroelastic model does not allow for variations in the mean wind speed inclination with height above terrain. Consequently a simplifying choice has to be made. In the present analysis it was decided to assume the mean wind speed inclination to vary linearly with altitude between the two observed values and to define the mean wind speed inclination as the inclination corresponding to the hub height. It was further decider to let the sector 1 values relate to the median of that sector (244°), and analogues to let the sector 2 values relate to the median of this sector (264°). The wind direction dependence is finally accounted for by interpolating linearly in the wind direction.

Speed up effect: The vertical mean wind profile including the speed up effect observed in [7] is assumed to scale linearly with the mean wind speed in analogy with the traditional logarithmic shear profiles.

Turbulence intensities: The magnitudes of σ_v/σ_u and σ_w/σ_u, respectively, are independent of the mean wind speed and have been set equal to 1.05 and 0.8, respectively.

Turbulence length scales: A Kaimal formulation of the turbulence spectrum is assumed. The length scales are specified as averages of the estimated turbulence length scales presented in Section 3.3 (700m for the longitudinal turbulence length scale, 375m for the lateral turbulence length scale and 200m for the transversal turbulence length scale).

Coherence: A slightly modified Davenport coherence model is assumed. The coherence decay factors have been specified to 12 for the longitudinal turbulence component, 7 for the lateral turbulence component and 5 for the transversal turbulence component.

Air mass density: For measurements performed in the summer period a mean air density equal to 0.998 kg/m^3 will be applied, and for measurements performed in the winter period a mean air density value equal to 1.060 kg/m^3 will be used in the simulations.

Gusts: Using constrained simulation, gusts with the amplitudes specified in Table 3.4-1 have been embedded in the synthetic turbulence field at the time where they appear in the physical wind speed time series. No observations of the gust centre are available and consequently the gust centre has been assumed to be positioned at the rotor centre.

4.6 Results

The simulated structural response corresponds to the measured quantities described in Table 3.3-2. Thus blade root moments have been determined at r=0.85m and main shaft moments have been evaluated at l=0.8m. The main shaft bending moments have subsequently been transformed to a non-rotating coordinate system to quantify the yaw and tilt loads.

The results from the performed simulations are presented in Appendix B (FLEX4 simulations) and in Appendix C (HawC simulations). To improve the clarity only load cases and signals that turned out to be substantially affected by the imposed gust loading have been presented.

As a consequence the edgewise blade bending moment, which is heavily dominated by the gravity loading has been omitted (except for the FLEX4 simulations). Furthermore, it was decided to let the rotating shaft bending moments be represented only by their transformed

counterparts described in the fixed coordinate system. Thus the analysis is restricted to blade flap moments, tilt and yaw moments and main shaft torsion moments. In addition the blade pitch angle signal is presented as the pitch behaviour is essential for the interpretation of resulting response signals.

In section 3 the gust load cases was organised "pair wise" in 4 different pitch operational classes - the low mean wind speed regime, the medium mean wind speed regime, the nominal mean wind speed regime and the high mean wind speed regime. For the analysed load cases, only the low wind regime, the medium wind regime and the high wind regime produced response signals with characteristics that could clearly be attributed to the imposed gust loading (which is also consistent with the measurements). For each of these classes, the particular load case that displays the most significant gust response have been chosen for presentation (load case 1, 6 and 8). In order to avoid influence from possible transients in the beginning of the simulation, and in addition to have a kind of reference load pattern associated with the wind field without the gust embedded, each simulation has been prescribed with an extension equal to 200 s in time.

5. Discussion

The *low wind regime* is characterized by an almost passive pitch system - cf. Figure C-5 and Figure D-5. The measured pitch regulation is, however, marginally more active then the pitch system implemented in the HawC model. In this operational regime, the turbine acts like a stall-regulated turbine in the linear aerodynamic regime. The flap bending moment and the shaft torsion moment are thus expected to increase with increasing wind speed – this behaviour is also observed around the gust event in both simulations and measurements (cf. Figures C-2, C-4, D-1 and D-4). No significant impact has been observed on the tilt nor on the yaw response. The explanation might be related to the fact that the gust was chosen to be positioned with its centre at the rotor centre, thus being rotational symmetric at the rotor plane. The simulated and measured signals are in good agreement qualitatively as well as quantitatively.

The *nominal and the high wind regimes* are characterized by an active pitch system – cf. the Figures B-1, B-2, C-10, C-15, D-10 and D-15. As the applied/measured turbulence fields are different realisations of basically the same stochastic process, the regulation patterns are not expected to be identical. However, the general "regulation range" should be similar, and specifically around the wind speed gust a quantitative agreement is required. These demands are seen to be satisfied by the present simulations and measurements. The pitch regulation primary adjusts the power output and thus the shaft torsional moment. Consequently, the shaft torsional moment is expected to be relatively unaffected by imposing a gust on the wind turbine provided that the time constant in the regulation algorithm is less that the gust rise time. This is also observed in the present simulations and measurements, as appears from Figures B-1, B-2, C-9, C-14, D-9 and D-14. As a consequence of the substantial pitch angle adjustment caused by the imposed wind gust, the flap bending moments are substantially reduced in the simulations as well as in the measurements. The observed reduction is of the order 50% - cf. the Figures B-1, B-2, C-7, C-12, D-6 and D-11. As with the low wind regime, no effect has been observed for the tilt and yaw responses neither in the simulations nor in the measurements. For some of the simulations there is even indications of a slightly reduced variation in these response signals associated with the gust loading, which might be attributed to a mechanism of replacing a number of small largely uncorrelated eddies with a much larger (symmetric located) and more coherent eddy.

Although not represented in the measured signals, the tower bottom bending moments caused primary by the thrust forcing have been analysed. For the low wind regime the gust

loading results in a 100% increase - for the nominal and high wind regime the increase is of the order 30%-40%.

In summary, the selected gust loading imposed on the investigated turbine turned out to result in only moderate changes of the response pattern compared to a load situation without the prescribed gust embedded. Thus none of the analysed gust load situations resulted in structural responses that could be characterized as extreme response situations. This is true for the measurements as well as for the performed simulations, which is mutually in good agreement.

There are a number of possible explanations for this observation:

• The selected type of wind speed gust can not be considered as a gust load for the particular wind turbine used in the present investigation;
• The observed gust amplitudes in the available measurements (which extended in only of the order two weeks) could not be characterized as an extreme amplitude;
• The selected position of the embedded gust is not critical for the loading;

The selected pitch regulated turbine seems to be able adjust the pitch angle fast enough to compensate for the increased wind speed caused by the present gust loading. The critical factor is probably the relation between the gust rise time and the time constant inherent in the regulation algorithm. However, the wind speed gradient tend to increase with increasing gust amplitude [1], and therefore larger gust amplitudes might result in load patterns that is critical also for the present turbine. Further, another wind climate with reduced turbulence length scale will also result in an autocorrelation function with increased gradient, and thus a gust formulation with larger wind gradient that might be potentially critical also to the present wind turbine. Finally, the gust position could be adjusted to obtain an increased impact. Investigations of this aspect have been performed in [13] and shows (for another wind turbine type) that some asymmetric positions of the gust centre is more critical than positioning the gust at the rotor centre.

The conducted analysis focuses primary on qualitative observations. A more extensive quantitative analysis will require a more comprehensive data material (with critical gusts represented) thus enabling the establishment of a distribution of extreme responses that can be compared with the similar distribution established from simulations based a number of realisations of basically the same stochastic process. In this connection it would be natural to extend the analysis also to stall regulated turbines.

6. Conclusions

The NewGust method has been verified by comparing existing measurements of wind speed gust situations, and associated structural loads on a Vestas V39 turbine, with analogues simulations achieved by using the NewGust method to establish a (synthetic) gust loading. The analysis has shown good agreement between the performed simulations and the measured responses, thus demonstrating that a constrained turbulence simulation can be performed and successively used as the load input to an aeroelastic model of the V39 turbine.

However, the gust loading selected for the study, and subsequently imposed on the investigated turbine, turned out to result in only moderate changes of the response pattern compared to a load situation without the prescribed gust embedded. Thus none of the analysed gust load situations resulted in structural responses that could be characterized as extreme response situations. The primary reason for that is that the available measured gust situations are related to gust rise times, which are somewhat larger then the time constant inherent in the pitch regulation of the turbine blades.

7. Acknowledgements

8. References

[1] Larsen, G.C., Bierbooms, W. and Hansen, K.S. (2000). Mean Gust Shapes. Risø-R-1133 (EN).

[2] Larsen, G.C., Bierbooms, W. and Hansen, K.S. (2000). Statistics of Local Extremes. Risø-R-1220(EN).

[3] Database on Wind Characteristics. http://www.winddata.com/

[4] Petersen, S.M. (1998). Investigation of Design Aspects & Design Options for Wind Turbines Operating in Complex Terrain Environments - Characterization of the Sky River Site. Internal work document prepared for the COMTERID JOULE project, Risø National Laboratory, Roskilde, Denmark.

[5] Petersen, S.M. (1998). Investigation of Design Aspects and Design Options for Wind Turbines Operating in Complex Terrain Environments - Measurement report; Vestas V39, Sky River. . Internal work document prepared for the COMTERID JOULE project, Risø National Laboratory, Roskilde, Denmark.

[6] Rich Simon (1989). "Evaluation of Wind Resource Potential". Zond System, INC, June 29.

[7] Thomsen, K. et. al (1996). Terrain Induced Loads on Pitch Regulated Wind Turbines. Risø-R-846 (EN).

[8] Panofsky, H.A. and Dutton, J.A. (1983). Atmospheric Turbulence - Models and methods for Engineering Applications. John Wiley & Sons.

[9] Petersen, S.M. and Larsen, G.C. (2000). Experimental investigation of extreme loads. Energistyrelsens Vindenergikonference, Billund, 30-31 May (in Danish).

[10] Petersen, J.T. (1990). Kinematically Non-linear Finite Element Model of a Horizontal Axis Wind Turbine. Part 1 and 2, . Risø National Laboratory, Roskilde, Denmark.

[11] Carlén, I. and Larsen, G.C. (2000). SOSIS-WG Input Deck Description.

[12] Øye, S. (1994) FLEX4 - Documentation (in Danish).

[13] P.W. Cheng, P.W and Bierbooms, W.A.A.M. (2000). Distribution of extreme gust loads of wind turbines. Submitted for publication in Journal of Wind Engineering and Industrial Aerodynamics.

[14] Bierbooms, W. and Dragt, J.B. (2000). A probabilistic method to determine the extreme response of a wind turbine. TU Delft, The Netherlands.

Appendix A: Selected time series

In the present appendix the selected time series for the NewGust verification are shown. The time series refer to wind speed measurements at hub height. Each time series is identified with the reference number introduced in Table 3.4-1, and the time for the occurrence of the identified extreme wind speed gust is furthermore specified.
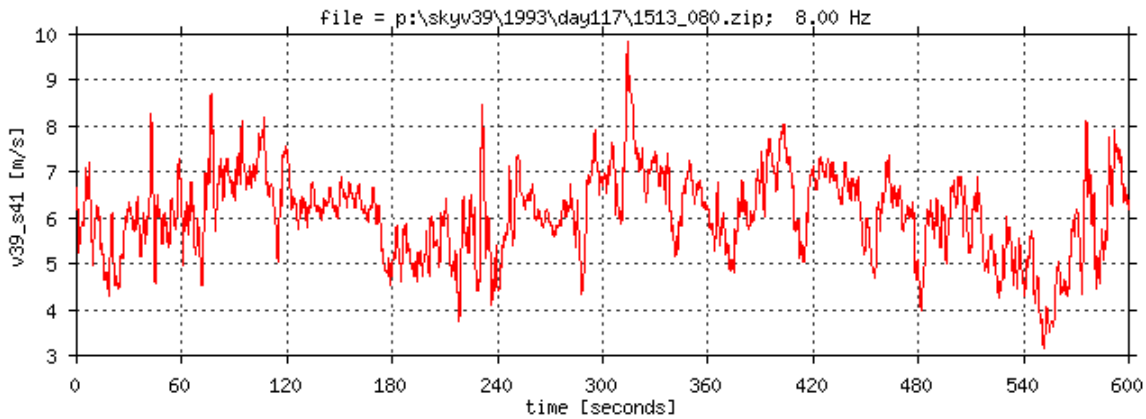
Figure A-1 Time series 1. Extreme gust occurrence at t = 314.13 s
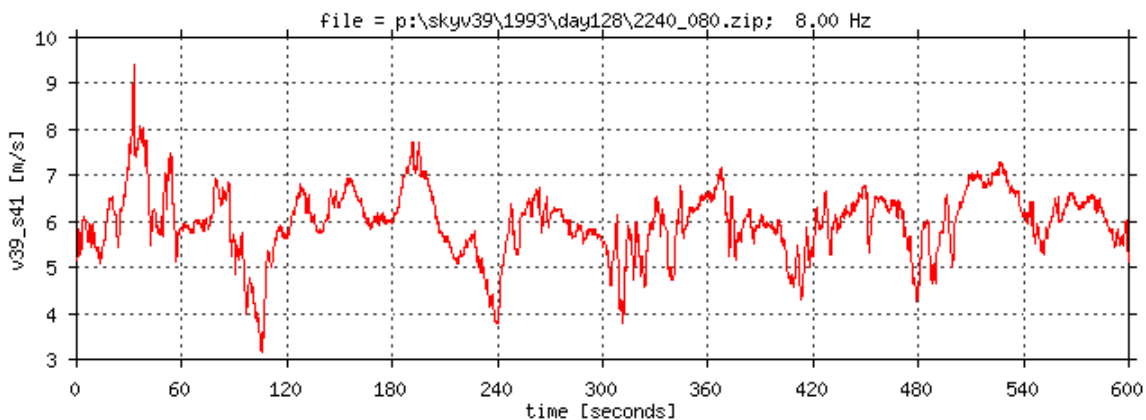
Figure A-2 Time series 2. Extreme gust occurrence at t = 32.50 s
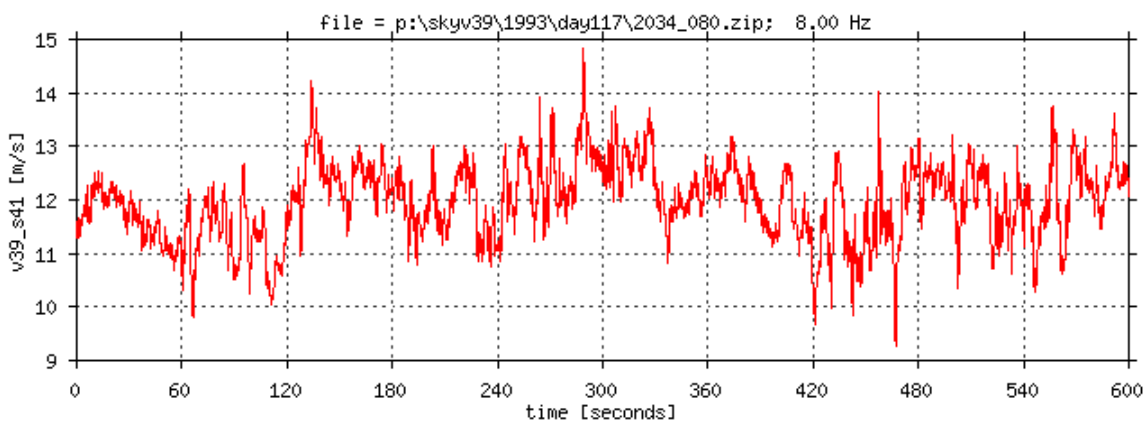
Figure A-3 Time series 3. Extreme gust occurrence at t = 288.94 s
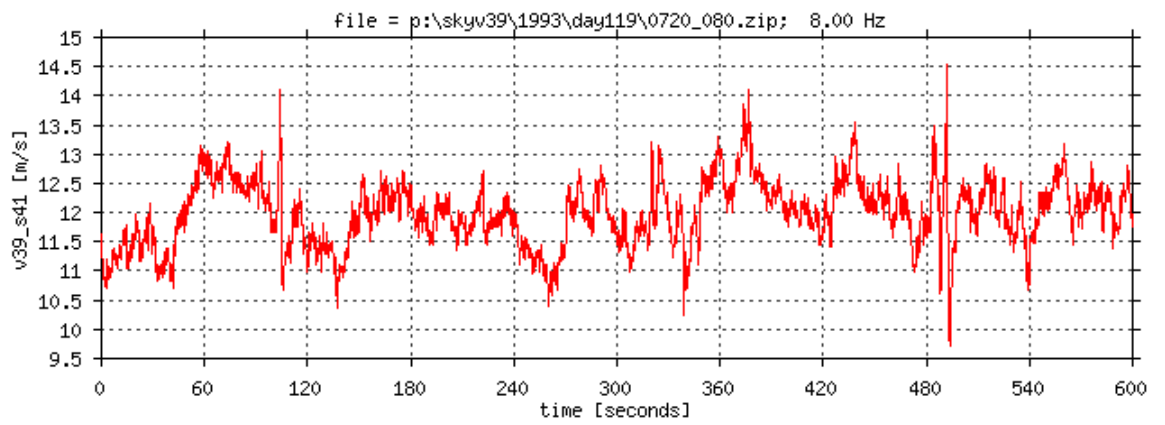
Figure A-4 Time series 4. Extreme gust occurrence at t = 492.00 s
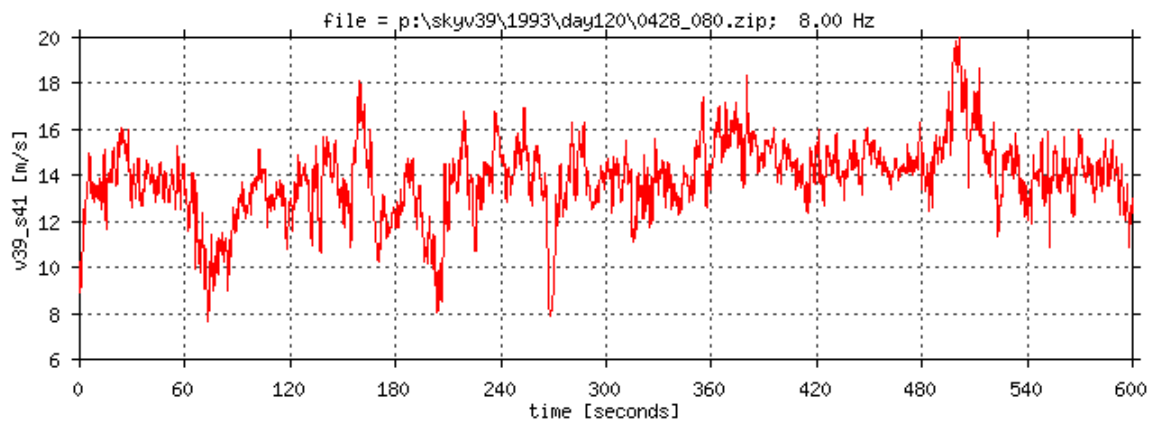
Figure A-5 Time series 5. Extreme gust occurrence at t = 501.12 s
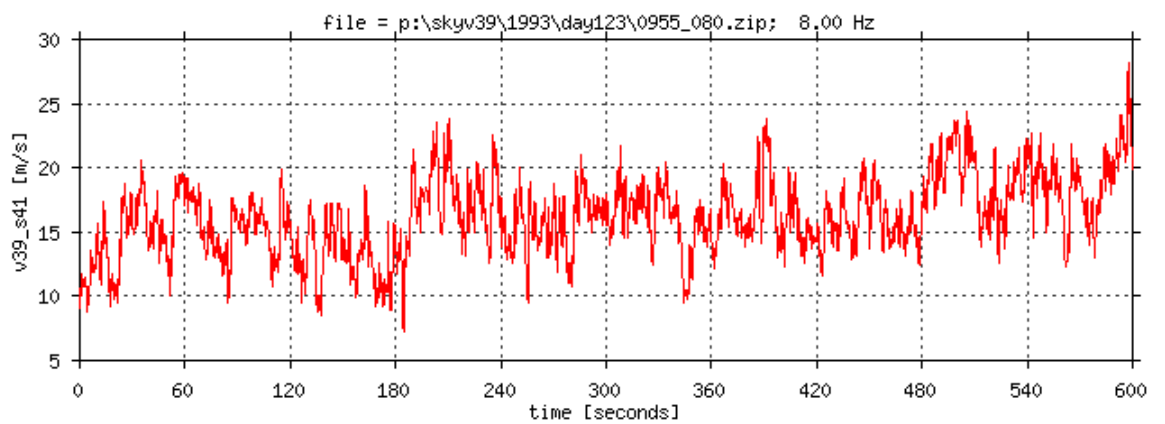
Figure A-6 Time series 6. Extreme gust occurrence at t = 597.87 s

file = p:\skyv39\1993\day120\2007_080.zip; 8.00 Hz
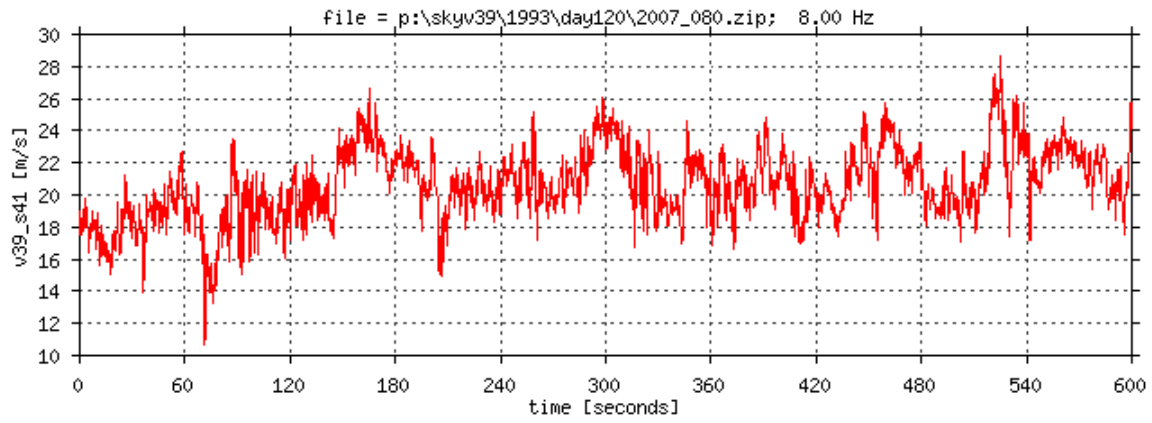
Figure A-7 Time series 7. Extreme gust occurrence at t = 525.20 s

file = p:\skyv39\1993\day123\0217_080.zip; 8.00 Hz
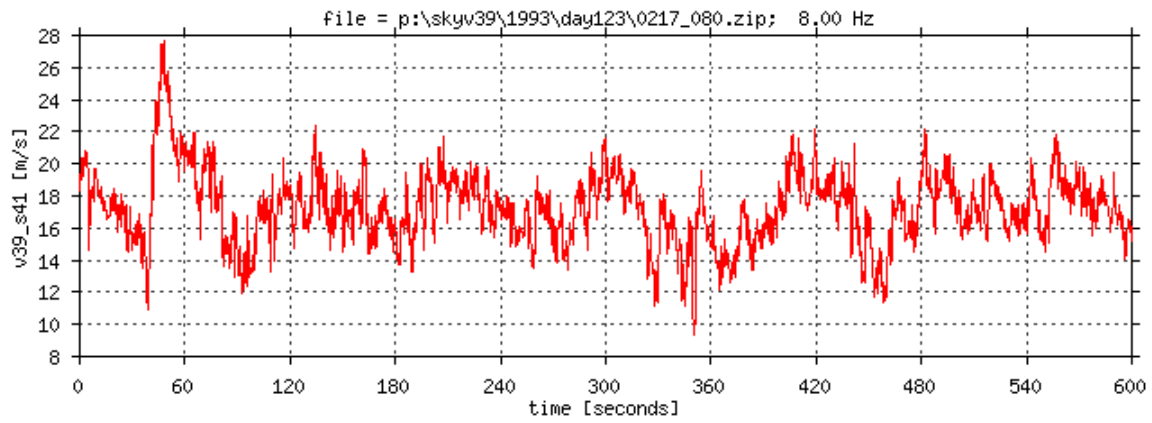
Figure A-8 Time series 8. Extreme gust occurrence at t = 48.12 s

Appendix B: FLEX4 results

The present appendix contains response time series resulting from the FLEX4 simulation of the selected gust load cases defined in Table 3.4-1. Only response signals in which the gust loading has a significant impact on the structural response are included (i.e. load case 6 and load case 8). Each gust situation is represented by a simulation extending 200s in time (with the gust centre at time 100s) in order to avoid any influence from possible transient behaviour at the beginning of the simulation.
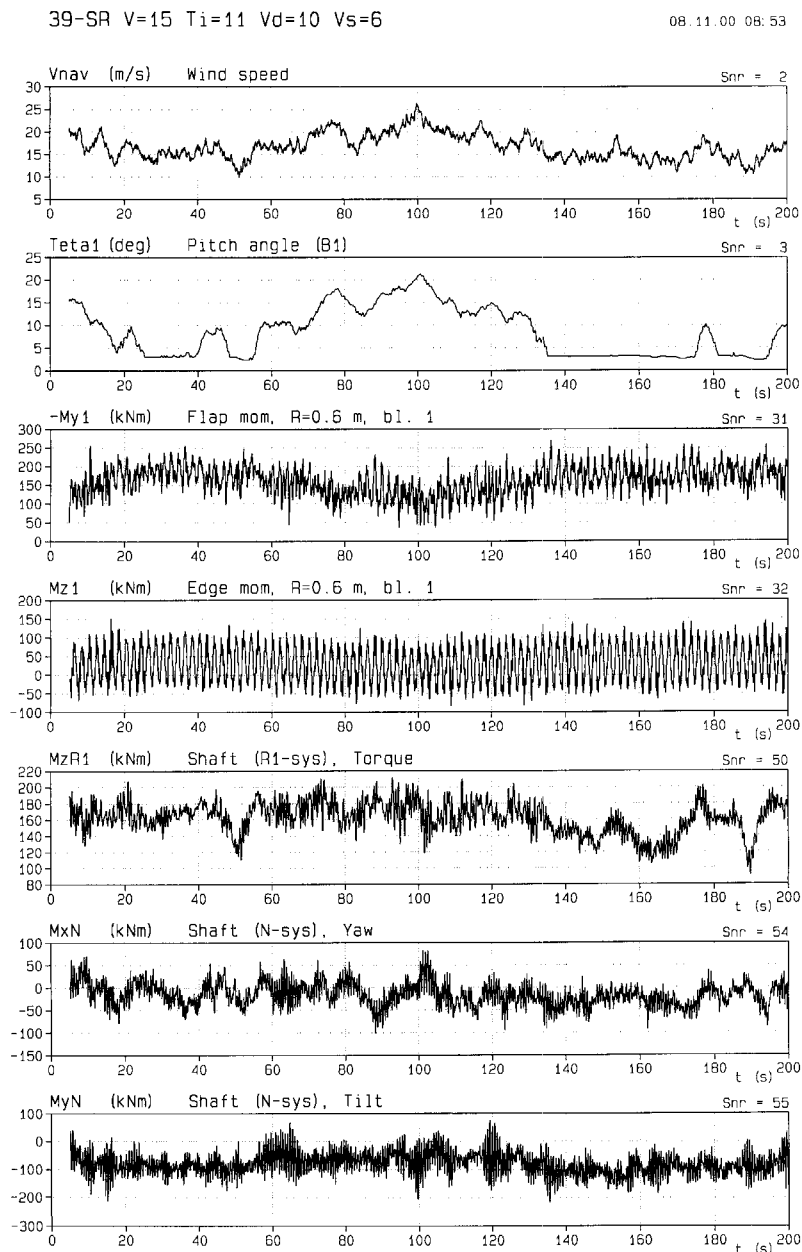
Figure B-1 Simulated wind speed and structural response corresponding to load case 6. Gust occurrence at t = 100 s.

2
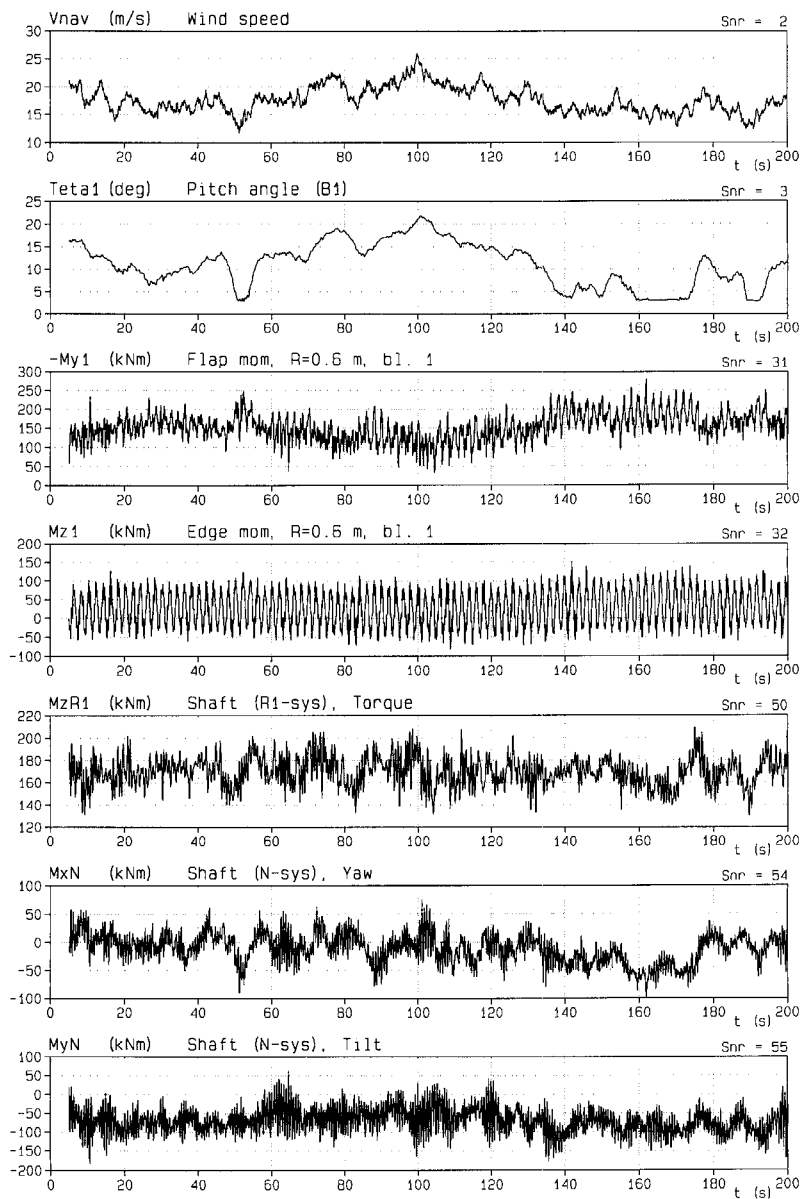
Figure B-2 Simulated wind speed and structural response corresponding to load case 8. Gust occurrence at t = 100 s.

Appendix C: HawC results

The present appendix contains response time series resulting from the HawC simulation of the selected gust load cases defined in Table 3.4-1. Only response signals in which the gust loading has a significant impact on the structural response are included (i.e. load case 1, 6 and 8). Each gust situation is represented by a simulation extending 200s in time (with the gust centre at time 100s) in order to avoid any influence from possible transient behaviour at the beginning of the simulation, which for tower bending signals might be of the order 40s.
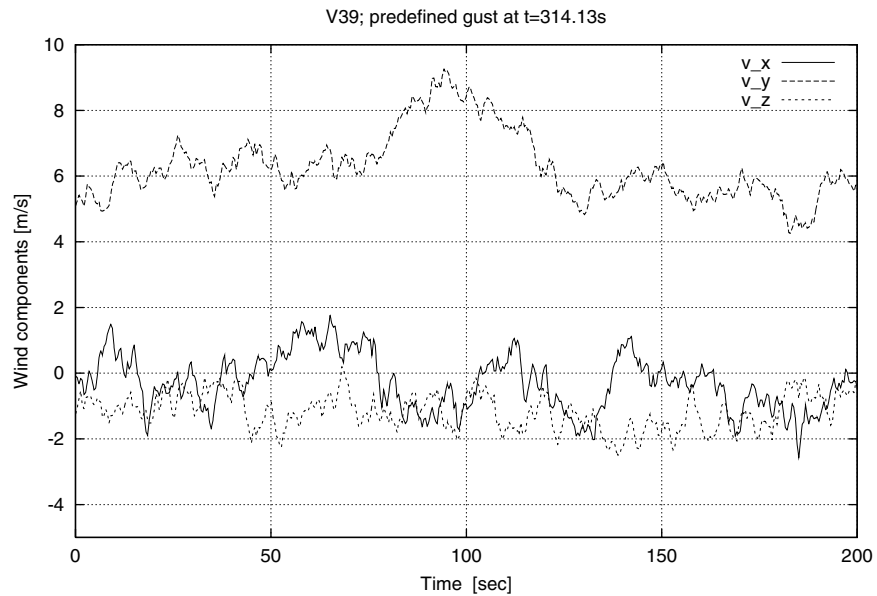
Figure C-1 Simulated wind field corresponding to load case 1. The gust centre is positioned at t = 100 s.
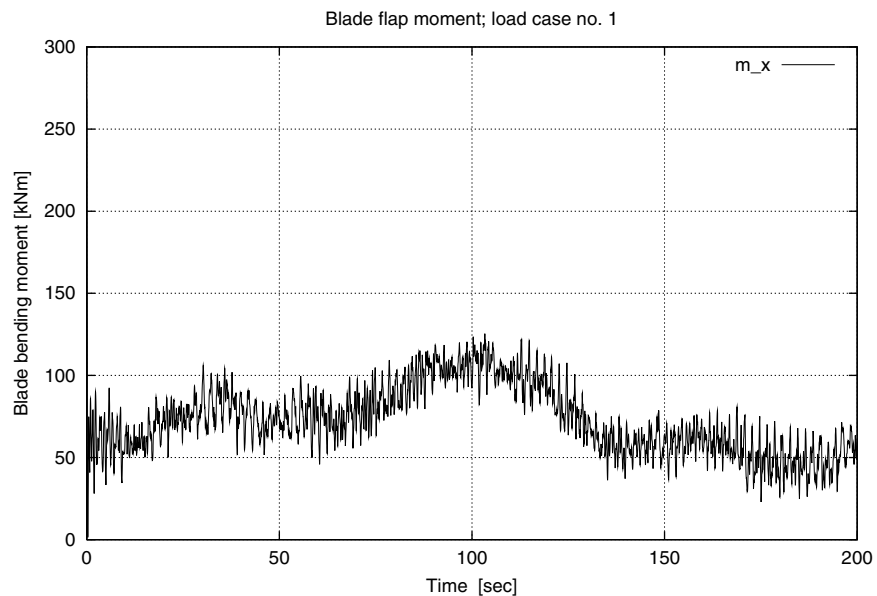
Figure C-2 Simulated flap response corresponding to load case 1. The gust centre is positioned at t = 100 s.
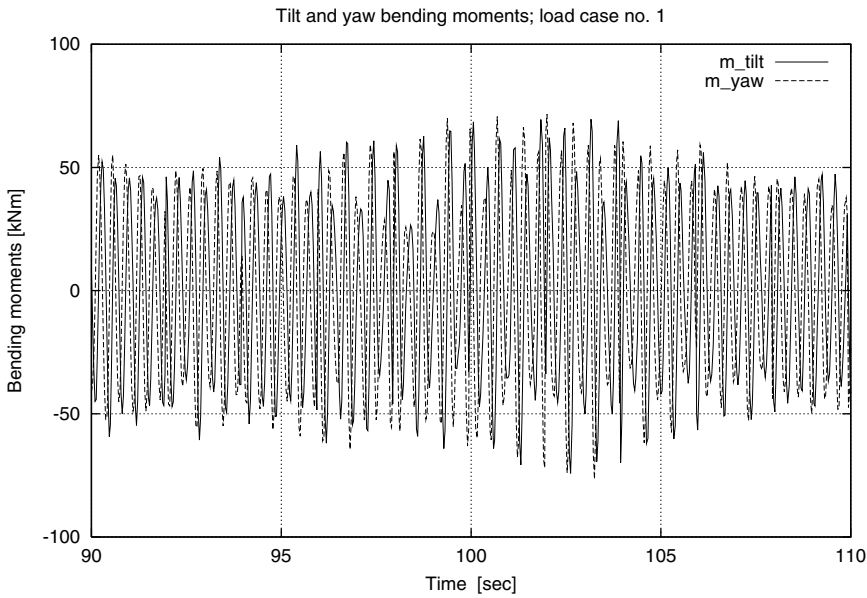
Figure C-3 Simulated tilt and yaw response corresponding to load case 1. The gust centre is positioned at t = 100 s.
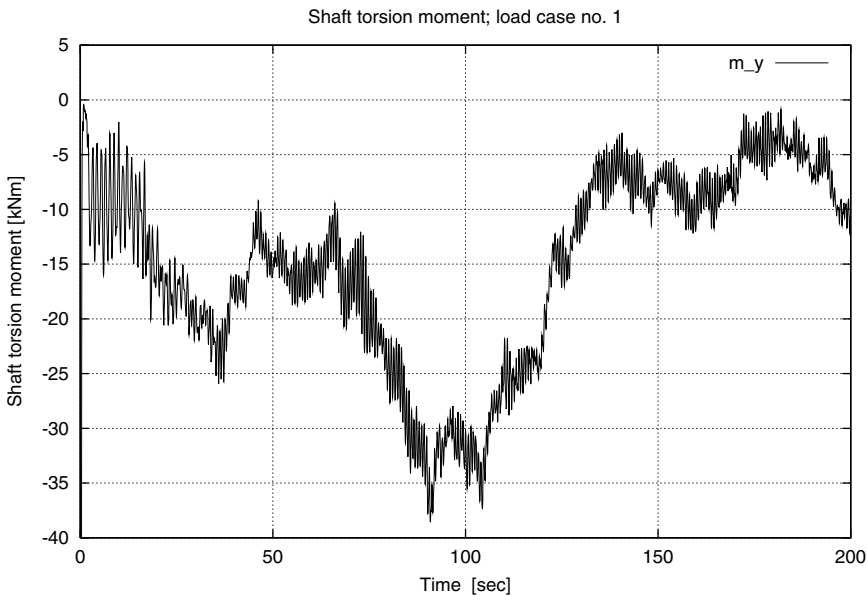
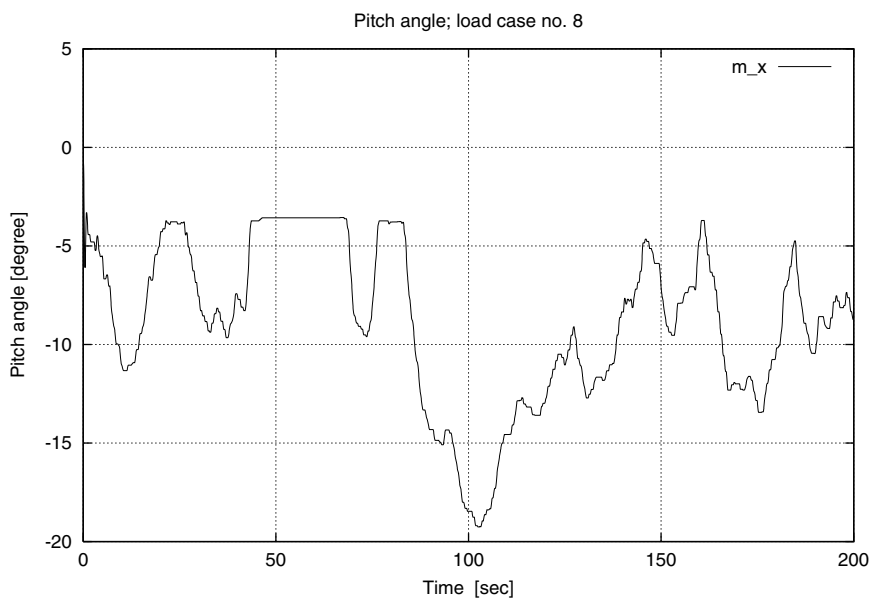**Figure C-4 Simulated shaft torsion response corresponding to load case 1. The gust centre is positioned at t = 100 s.**
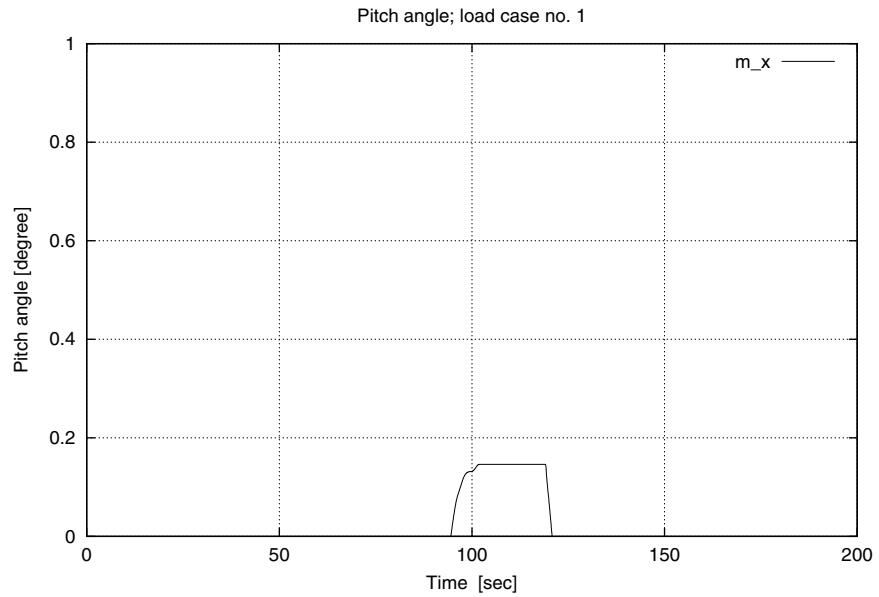
Figure C-5 Simulated pitch angle corresponding to load case 1. The gust centre is positioned at t = 100 s.
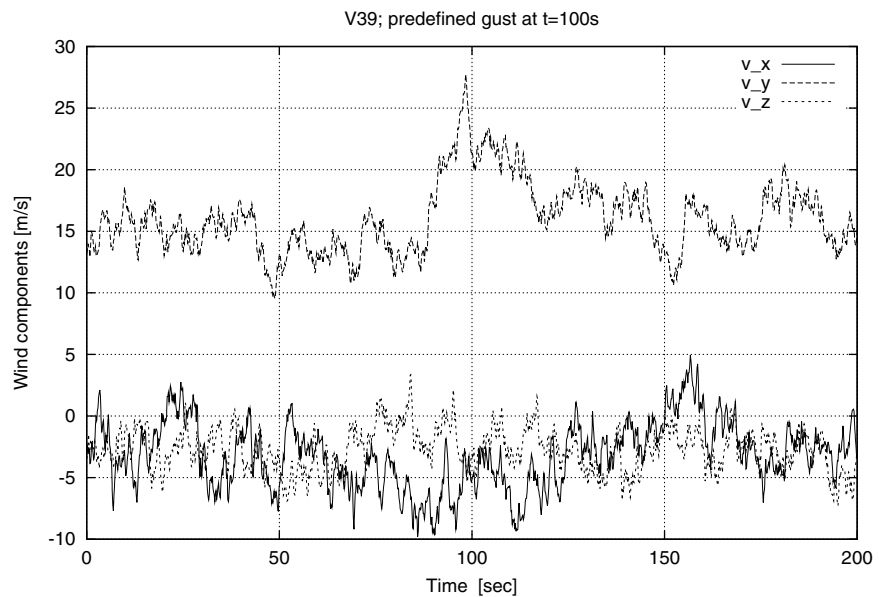
Figure C-6 Simulated wind field corresponding to load case 6. The gust centre is positioned at t = 100 s.
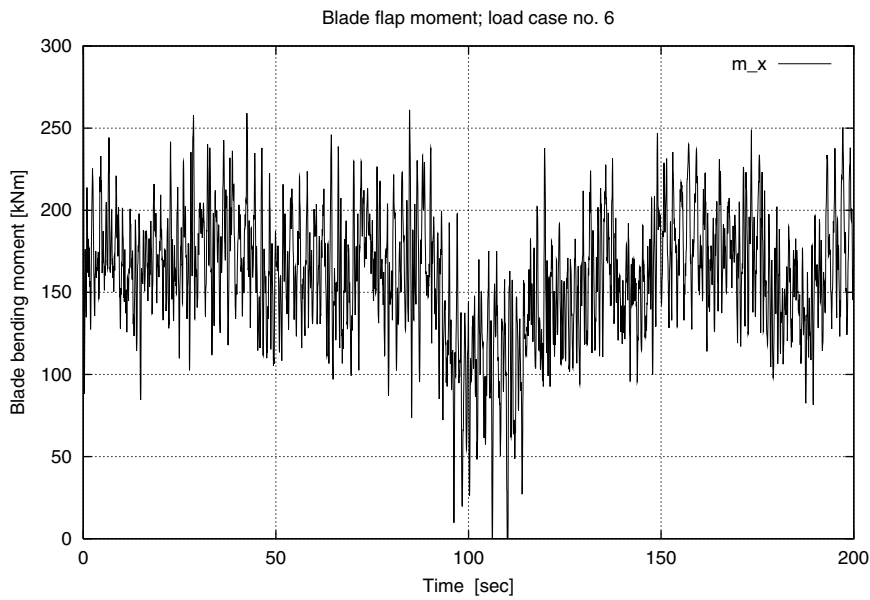
Figure C-7 Simulated flap response corresponding to load case 6. The gust centre is positioned at t = 100 s.
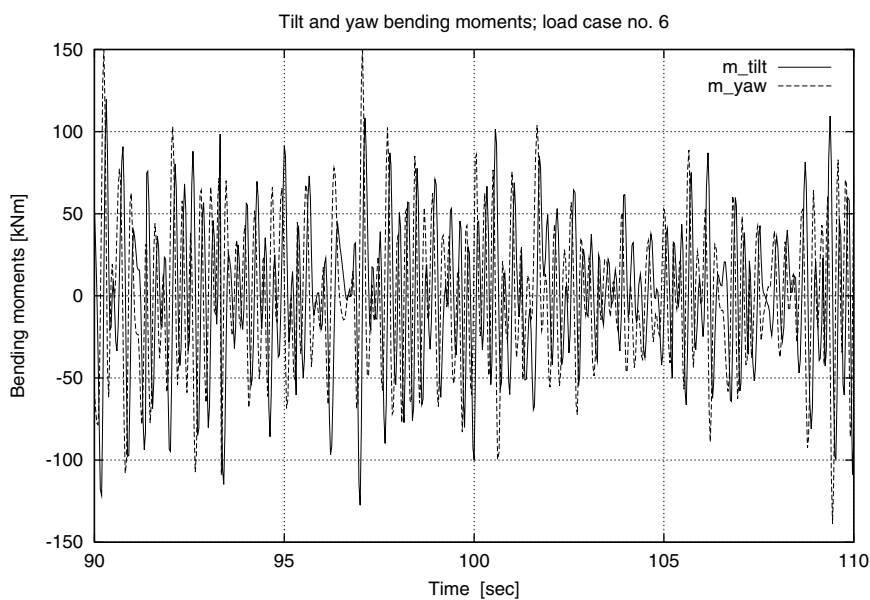
Figure C-8 Simulated tilt and yaw response corresponding to load case 6. The gust centre is positioned at t = 100 s.
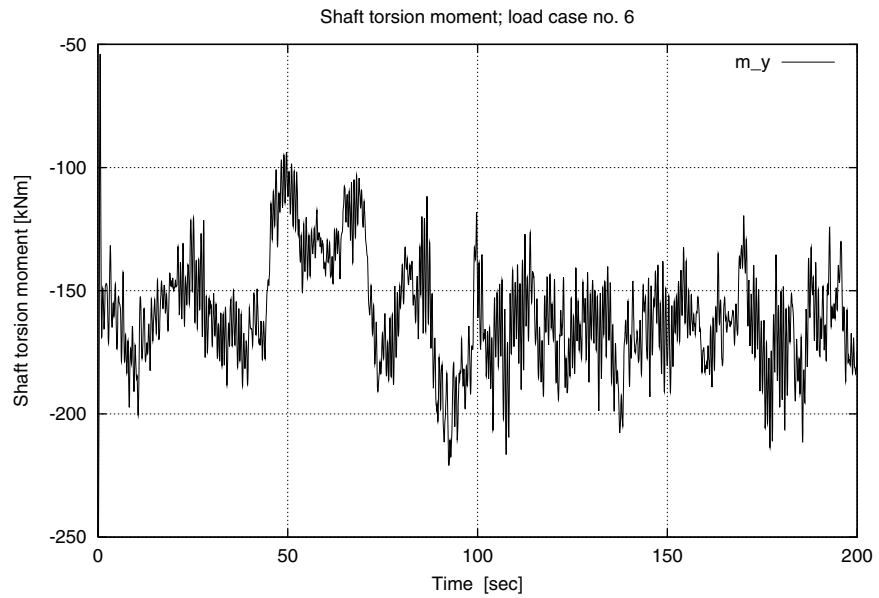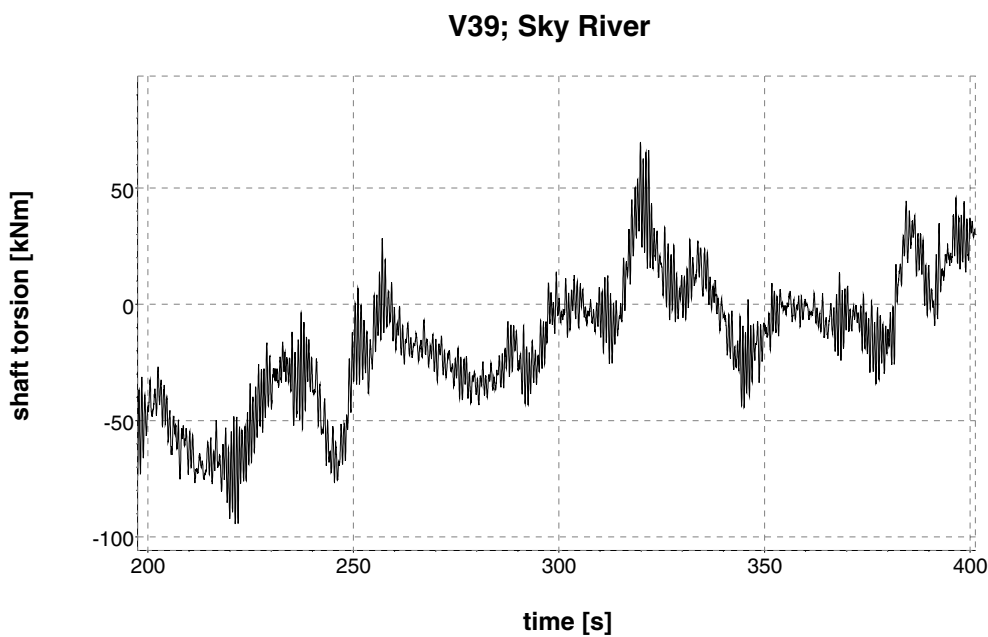
Figure C-9 Simulated shaft torsion response corresponding to load case 6. The gust centre is positioned at t = 100 s.
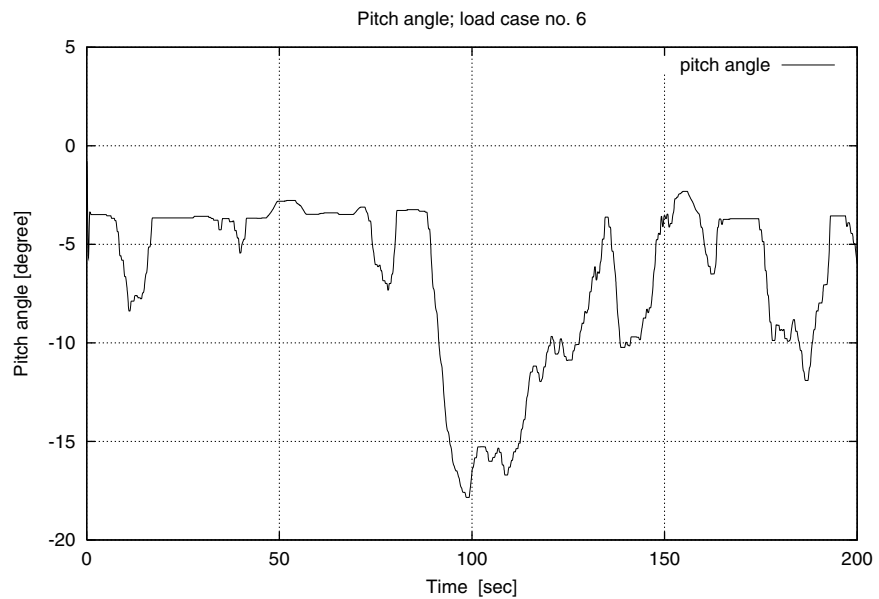
Figure C-10 Simulated pitch angle corresponding to load case 6. The gust centre is positioned at t = 100 s.

V39; predefined gust at t=100s
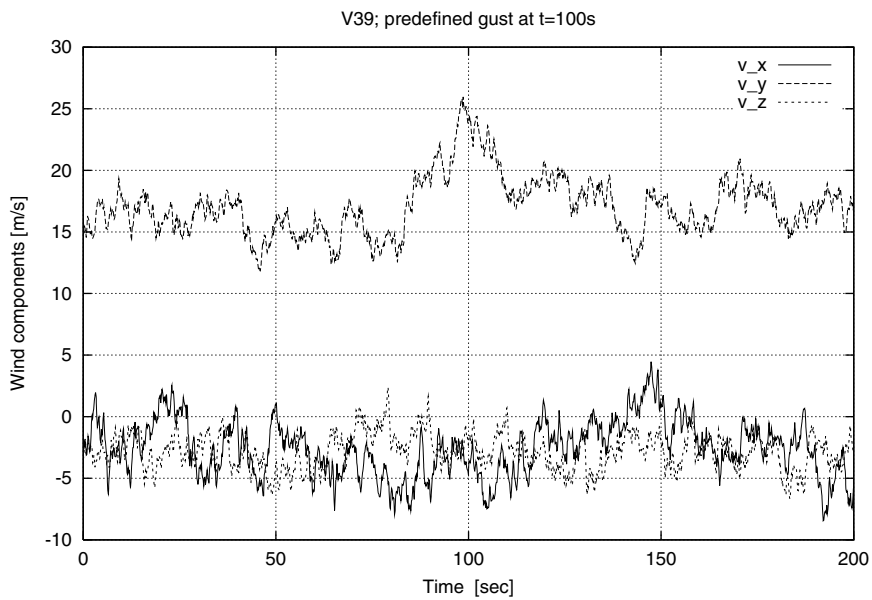
Figure C-11 Simulated wind field corresponding to load case 8. The gust centre is positioned at t = 100 s.

Blade flap moment; load case no. 8
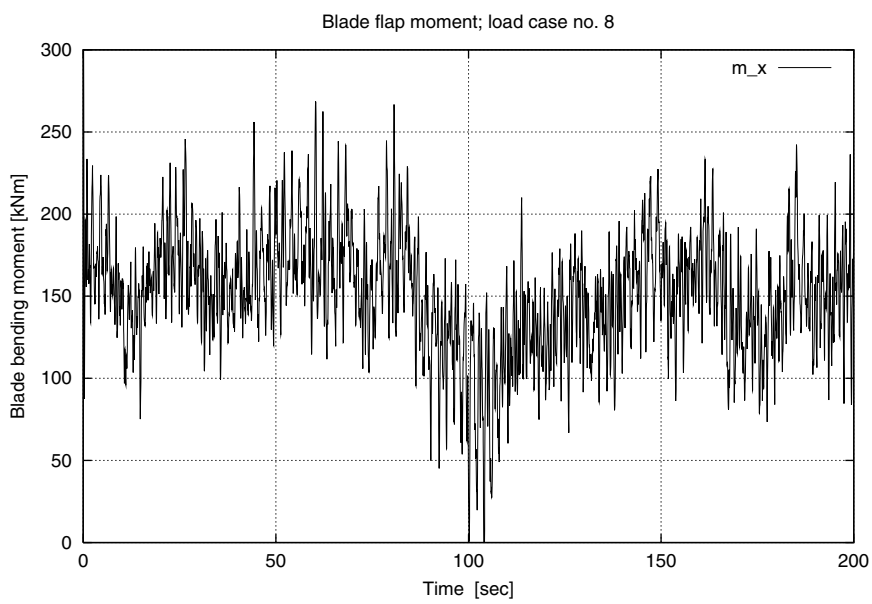
Figure C-12 Simulated flap response corresponding to load case 8. The gust centre is positioned at t = 100 s.
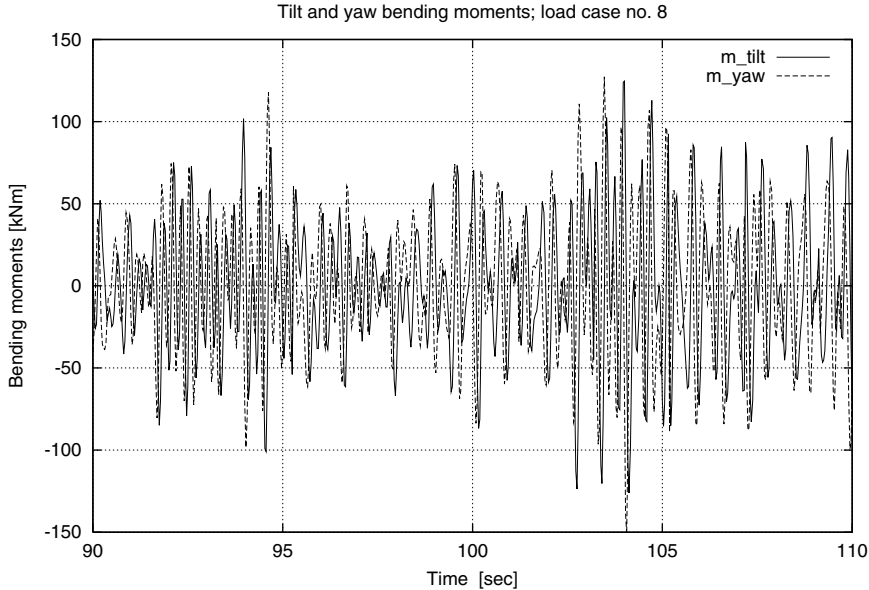
Figure C-13 Simulated tilt and yaw response corresponding to load case 8. The gust centre is positioned at t = 100 s.
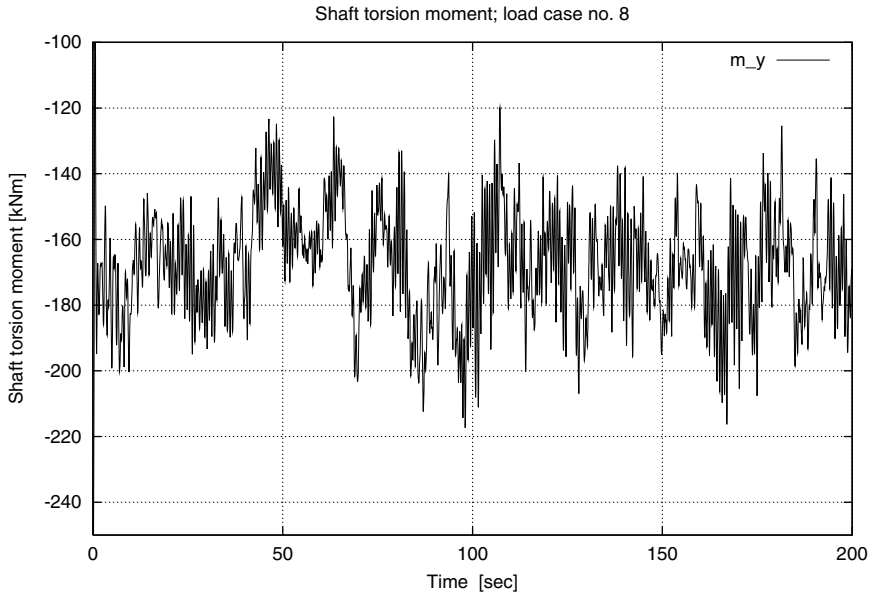
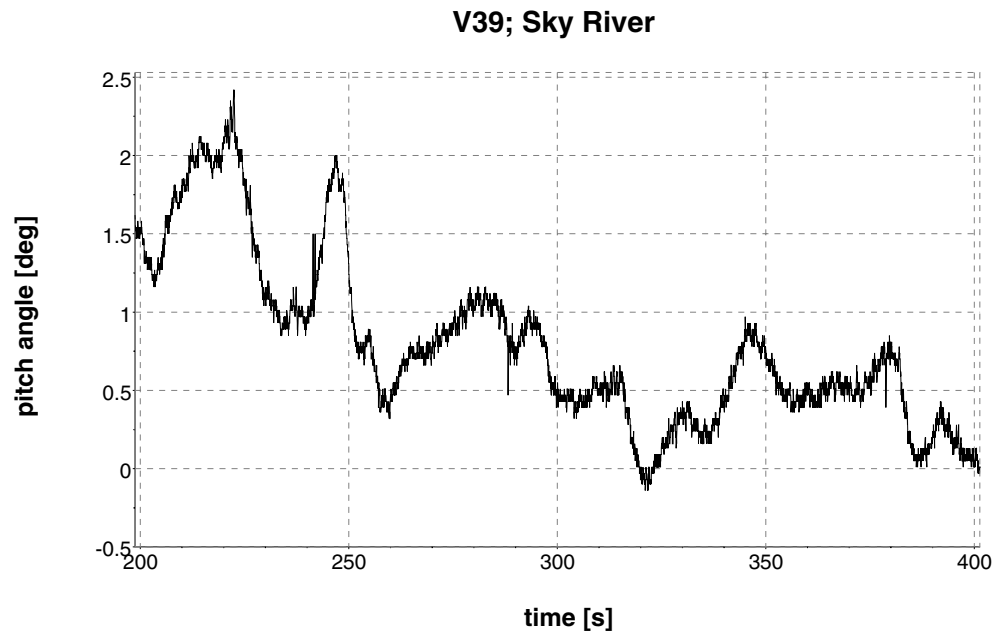**Figure C-14 Simulated shaft torsion response corresponding to load case 8. The gust centre is positioned at t = 100 s.**

**Figure C-15 Simulated pitch angle corresponding to load case 8. The gust centre is positioned at t = 100 s.**

Appendix D: Measured V39 responses

The present appendix contains time series corresponding to the V39 response measurements associated with the selected gust load cases defined in Table 3.4-1. Only response signals in which the gust loading has a significant impact on the structural response are included (i.e. load case 1, 6 and 8). In order to ease the comparison with the simulations, each gust situation is represented by a measurement record extending 200s in time.

V39; Sky River
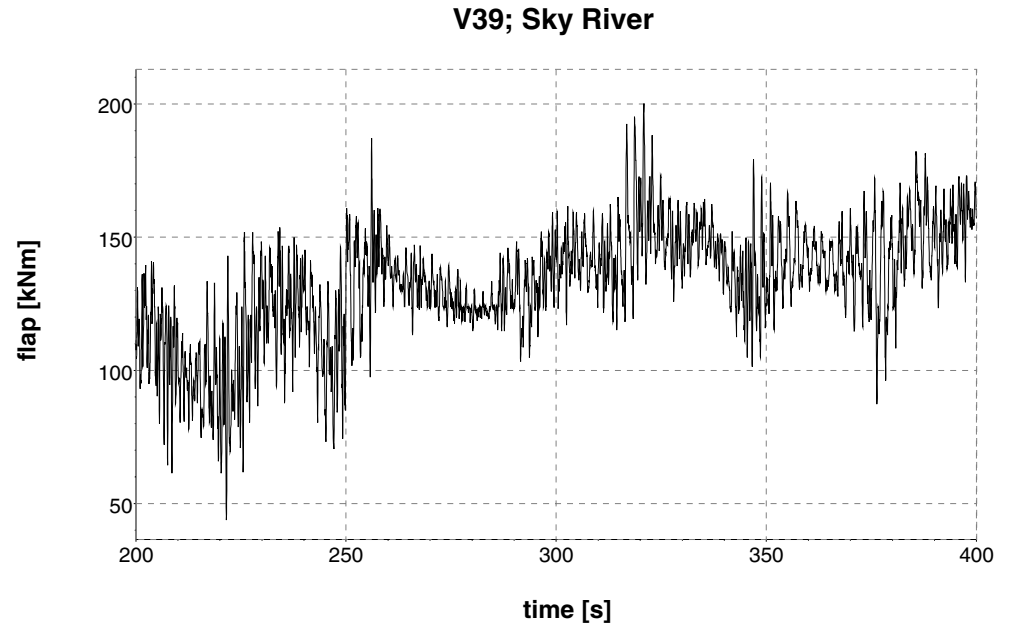
Figure D-1 Measured flap response corresponding to load case 1. The gust centre is positioned at t = 314.1 s.
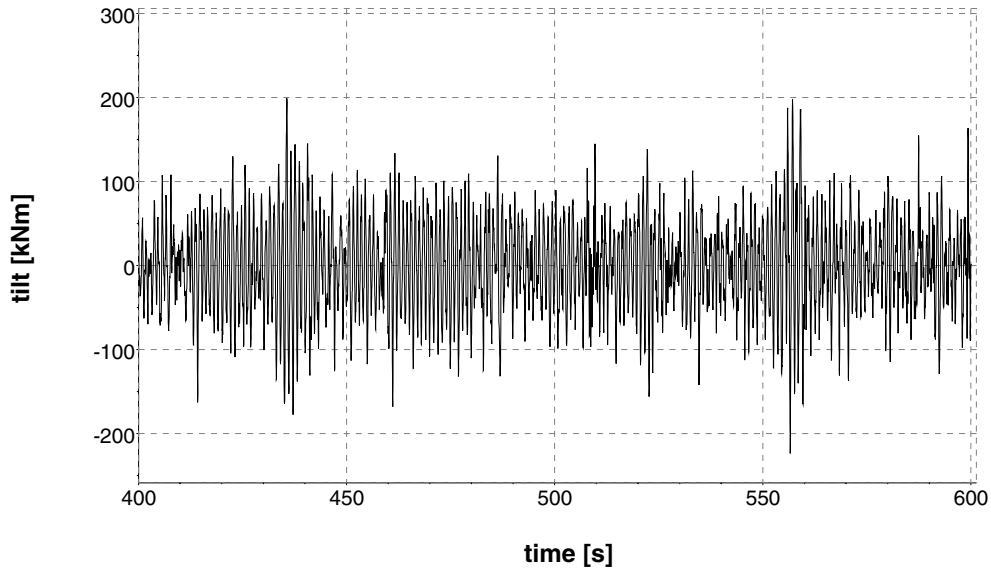
V39; Sky River
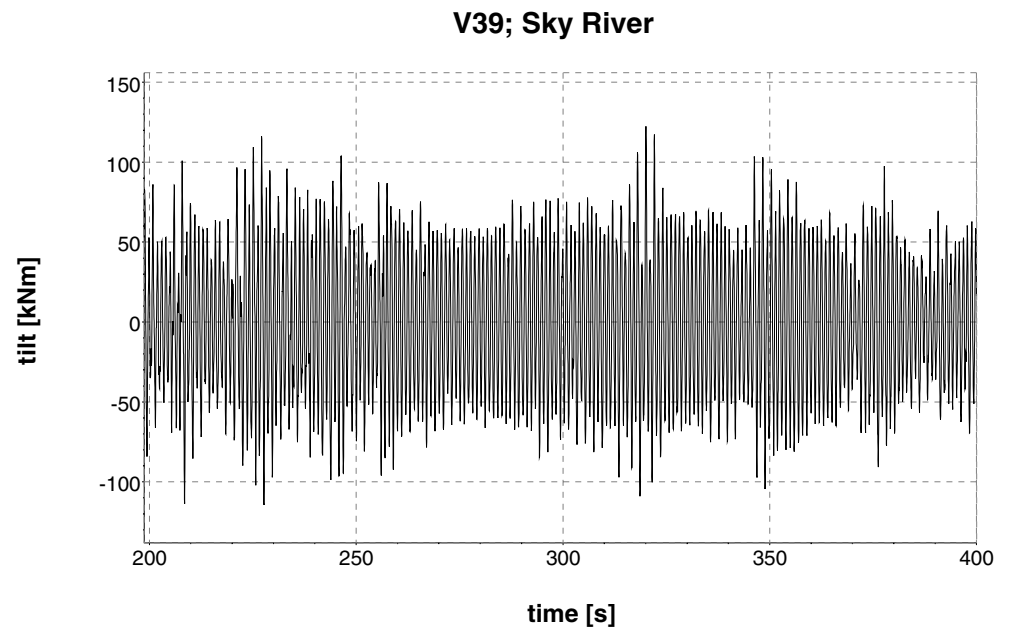
Figure D-2 Measured tilt response corresponding to load case 1. The gust centre is positioned at t = 314.1 s.
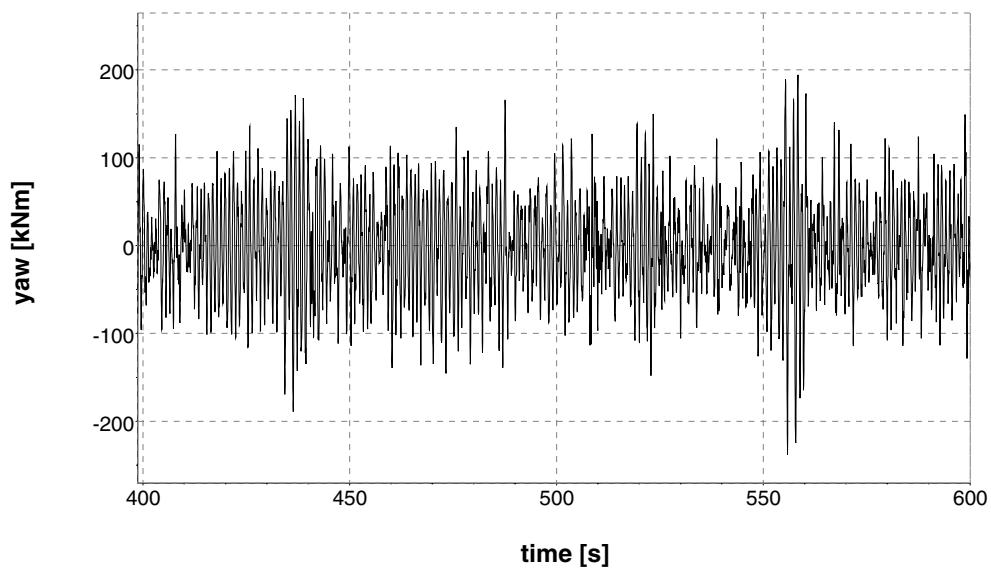

V39; Sky River
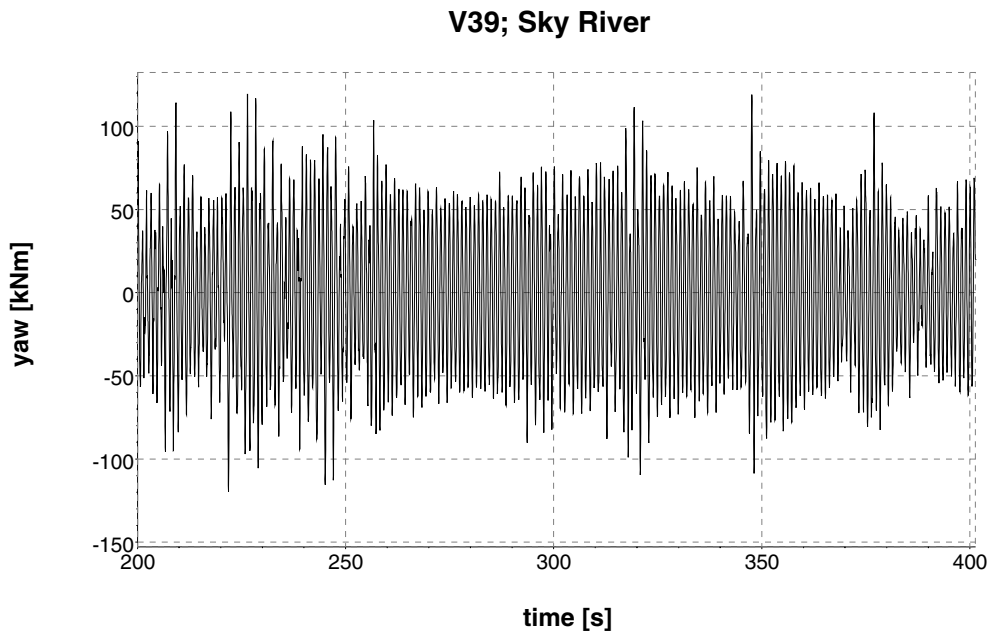
Figure D-3 Measured yaw response corresponding to load case 1. The gust centre is positioned at t = 314.1 s.
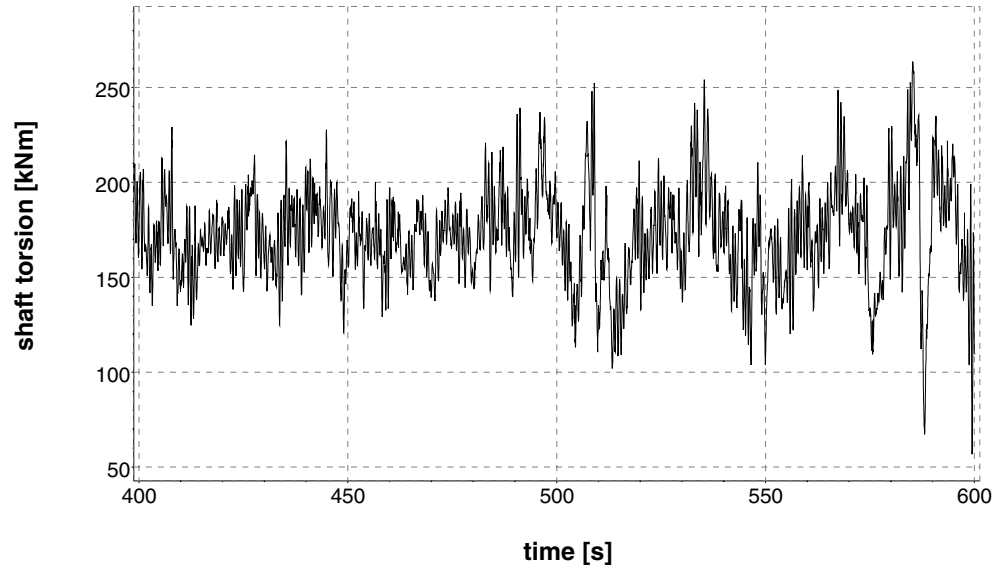

V39; Sky River

Figure D-4 Measured shaft torsion response corresponding to load case 1. The gust centre is positioned at t = 314.1 s.
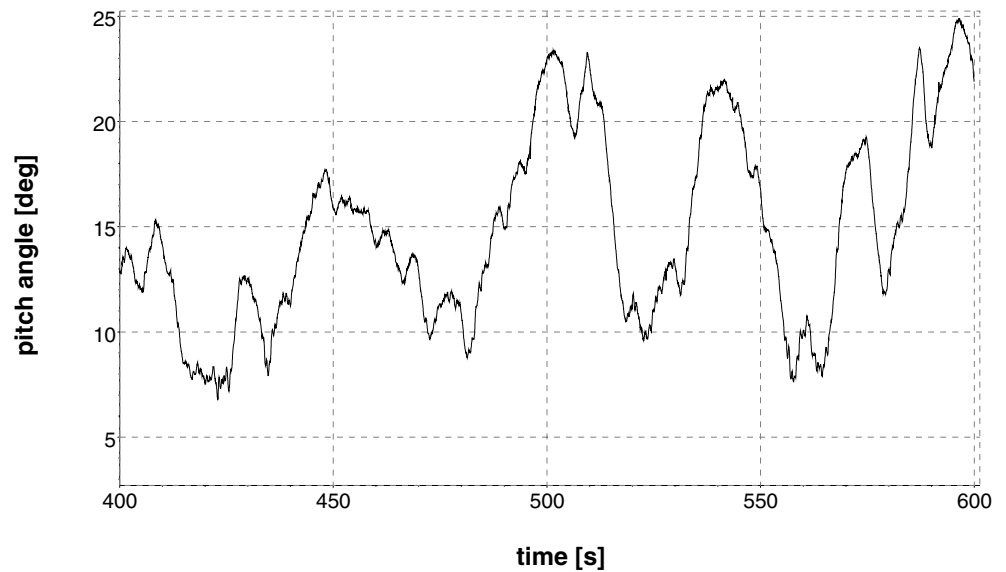
V39; Sky River

Figure D-5 Measured pitch angle corresponding to load case 1. The gust centre is positioned at t = 314.1 s.
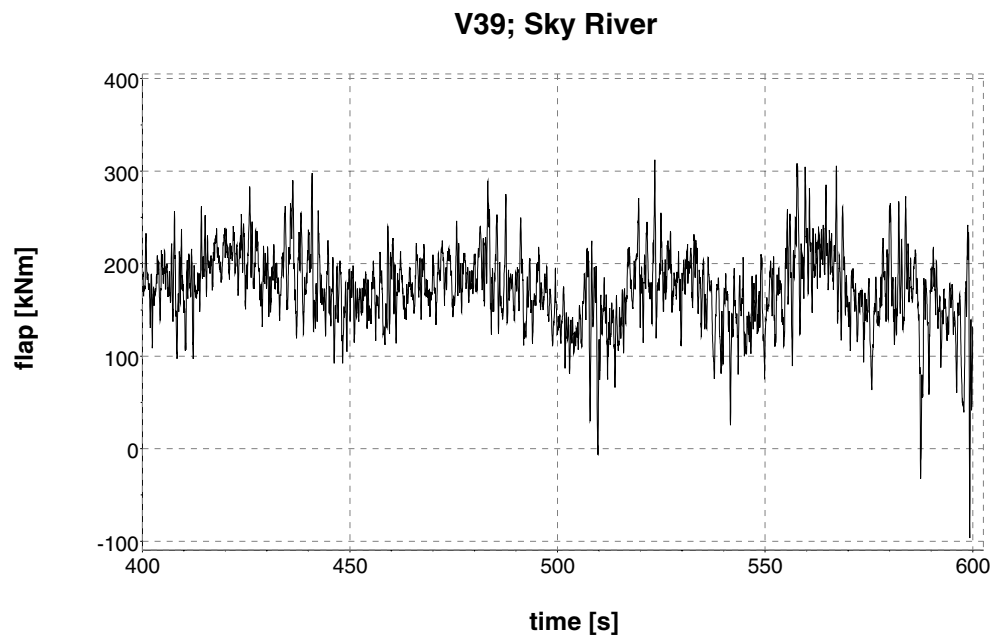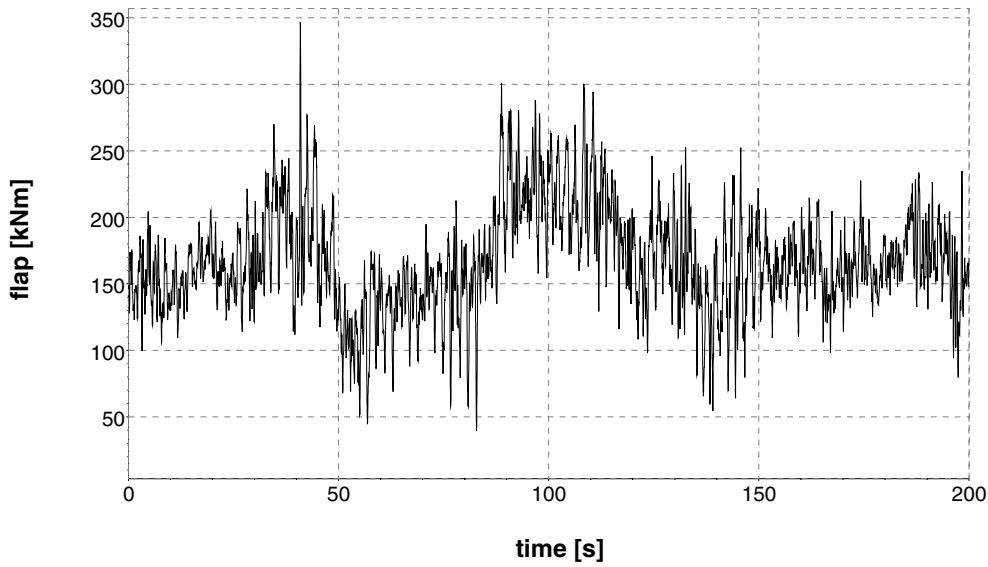
V39; Sky River

Figure D-6 Measured flap response corresponding to load case 6. The gust centre is positioned at t = 597.9 s.

V39; Sky River

Figure D-7 Measured tilt response corresponding to load case 6. The gust centre is
positioned at t = 597.9 s.

V39; Sky River

Figure D-8 Measured yaw response corresponding to load case 6. The gust centre is
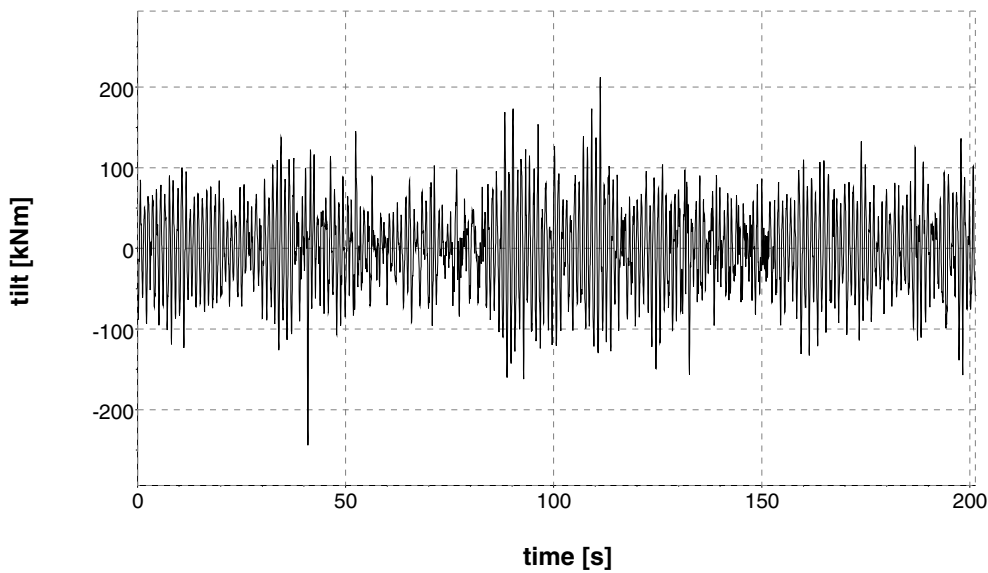positioned at t = 597.9 s.

V39; Sky River

Figure D-9 Measured shaft torsion response corresponding to load case 6. The gust centre is positioned at t = 597.9 s.

V39; Sky River

Figure D-10 Measured pitch angle corresponding to load case 6. The gust centre is positioned at t = 597.9 s.

V39; Sky River

Figure D-11 Measured flap response corresponding to load case 8. The gust centre is positioned at t = 48.1 s.

V39; Sky River

Figure D-12 Measured tilt response corresponding to load case 8. The gust centre is positioned at t = 48.1 s.
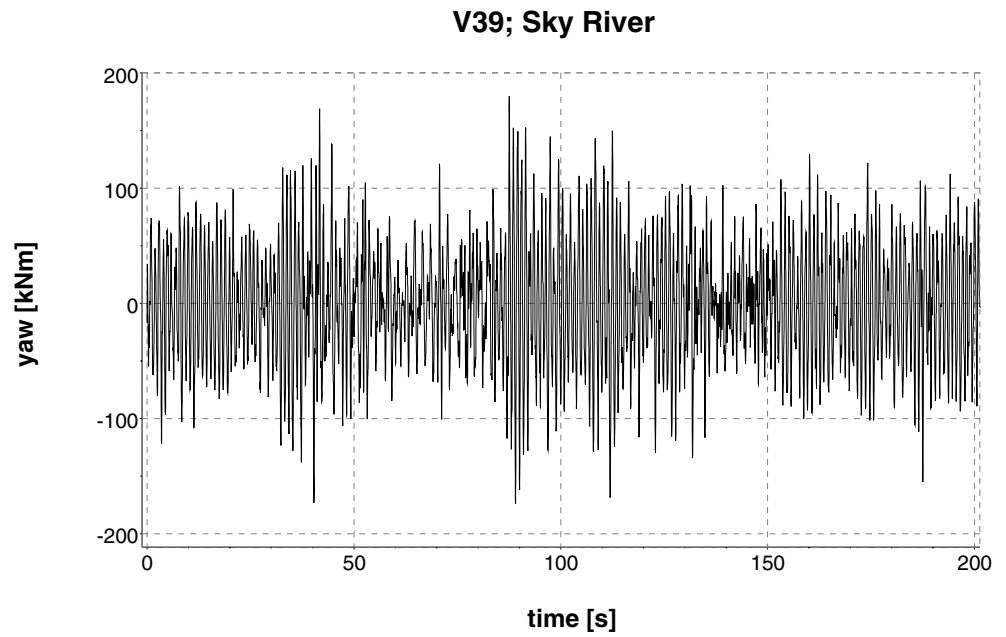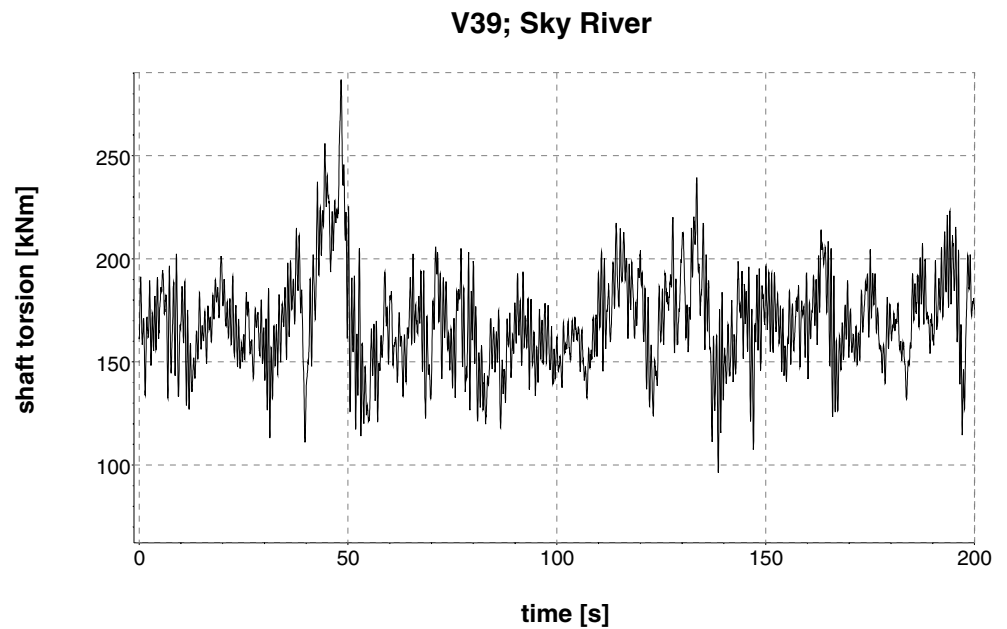
V39; Sky River

Figure D-13 Measured yaw response corresponding to load case 8. The gust centre is positioned at t = 48.1 s.

V39; Sky River

Figure D-14 Measured shaft torsion response corresponding to load case 8. The gust centre is positioned at t = 48.1 s.
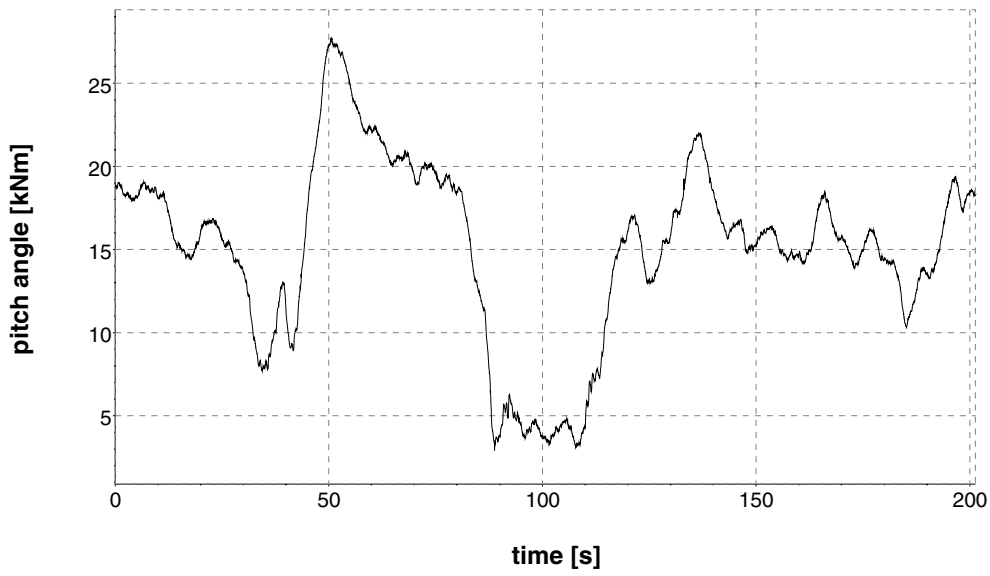
V39; Sky River

Figure D-15 Measured pitch angle corresponding to load case 8. The gust centre is positioned at t = 48.1 s.

The gust events described in the IEC-standard are formulated as coherent gusts of an inherent deterministic character, whereas the gusts experienced in real situation are of a stochastic nature with a limited spatial extension. This conceptual difference may cause substantial differences in the load patterns of a wind turbine when a gust event is imposed.

Methods exist to embed a gust of a prescribed appearance in a stochastic wind field in a consistent way. The present report deals with the verification of a synthetic wind field resulting from such a model - the NewGust model. The NewGust model is restricted to gust events associated with the longitudinal turbulence component, and consequently no attention is paid to wind direction gusts.

The verification is performed by analysing existing measurements of wind speed gust situations and associated structural loads on a Vestas V39 turbine, and subsequently to compare these with analogues simulations applying the NewGust method in order to establish a (synthetic) gust loading. Eight load cases, representing four mean wind speed regimes that reflect different control characteristics, have been analysed. Attention has been paid to select the largest possible gust events, associated with each of the mean wind ranges, within the available data material.

The work reported makes part of the project "Modelling of Extreme Gusts for Design Calculations " (NEWGUST), which is co-funded through JOULEIII on contract no. JOR3-CT98-0239.